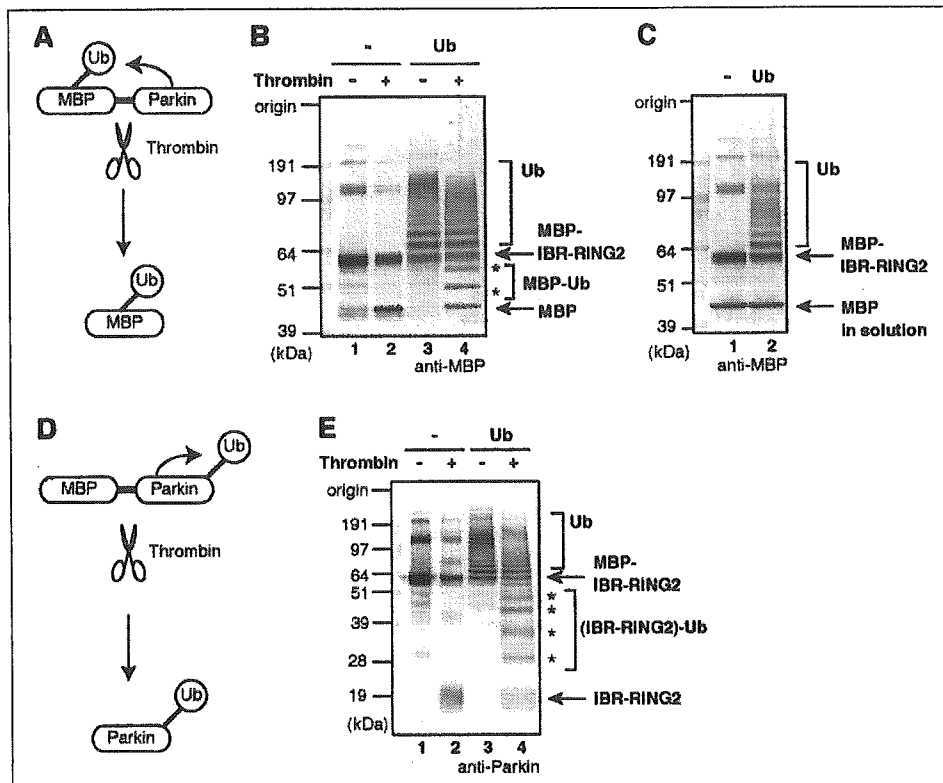


## Parkin Catalyzes Multiple Monoubiquitylation *In Vitro*

**FIGURE 2. In-frame-fused MBP can be a good pseudosubstrate of Parkin.** *A*, a schematic diagram of Parkin catalyzed ubiquitylation of MBP. If the MBP portion is ubiquitylated, a change in its mobility would be recognized by immunoblotting after cleavage. *B*, the MBP-(IBR-RING2) fused protein (see Fig. 4) was subjected to *in vitro* ubiquitylation, subsequent cleavage into MBP moiety, and immunoblotting with anti-MBP antibody. The MBP portion of IBR-RING2 was ubiquitylated (asterisks). *C*, MBP can be ubiquitylated only when it is in the physical vicinity of Parkin. Note that free MBP in solution was not ubiquitylated. *D*, a schematic diagram of Parkin-catalyzed autoubiquitylation. *E*, IBR-RING2 portion is also ubiquitylated. Asterisks in lane 4 show the ubiquitylated IBR-RING2 moiety (compare lane 4 with 2). Ubc7 was used as E2 in these experiments.



activity than GST-Parkin, as shown in Fig. 1F, we used MBP-Parkin in the following experiments.

**Fused MBP Is a Good Pseudo-substrate to Monitor E3 Activity of Parkin**—We next determined whether the MBP portion or Parkin portion (or both) is ubiquitylated. To check this, we purified MBP-LVPRGS-Parkin, in which a thrombin-digestion sequence is inserted between MBP and Parkin. As depicted in Fig. 2A, if the MBP moiety is ubiquitylated, its molecular weight would increase by ubiquitylation and subsequent digestion, but if not ubiquitylated, its molecular weight would remain unchanged. First we tried to split MBP-LVPRGS-Parkin by thrombin; however, this recombinant protein was hardly digested for some unknown reason (data not shown). We next fused the C-terminal IBR-RING2 region of Parkin to MBP-LVPRGS (hereafter dubbed IBR-RING2, see Fig. 4A), and this construct was cleaved moderately (Fig. 2B, lanes 1 and 2). When IBR-RING2 was subjected to an ubiquitylation assay and subsequently separated into MBP and IBR-RING2 portions by thrombin digestion, the molecular weight of MBP moiety was clearly increased (see the asterisks in Fig. 2B, lanes 3 and 4), meaning that the MBP portion is ubiquitylated. Does this result mean that bacterial MBP protein is the substrate for Parkin? The answer is no. When sole MBP protein was incubated with IBR-RING2, this free MBP was not ubiquitylated at all, even though IBR-RING2 was autoubiquitylated as described (Fig. 2, compare C with B). This result indicates that the IBR-RING2 region of Parkin ubiquitylates fused-MBP, but not unbound MBP, and strongly suggests that Parkin recognizes MBP as a substrate not because of its amino acid sequence but because of its physical vicinity to Parkin. As depicted in Fig. 2D, when the same experiment was repeated using an anti-Parkin antibody, the molecular weight of the IBR-RING2 moiety was also increased meaning that both MBP and IBR-RING2 portions were ubiquitylated (Fig. 2E). Although many putative substrates of Parkin have been reported, the lack of a good *in vitro* substrate makes any biochemical study difficult. Our study revealed that

fused MBP could be a good pseudo-substrate to monitor the E3 activity of Parkin.

**Parkin by Itself Catalyzes Multiple Monoubiquitylation**—The Uev1-Ubc13 heterodimer is an E2 involved in the formation of Lys-63-linked polyubiquitylation (19). We confirmed that our Uev1-Ubc13 complex is functional (Fig. 1D and supplemental Fig. 1A). Motivated by the findings that Parkin catalyzes Lys-63-linked polyubiquitylation (20, 21) and Parkin cooperates with Uev1-Ubc13 in our assay (Fig. 1B), we investigated the mode of Parkin-catalyzed ubiquitylation. Parkin could either catalyze multiple monoubiquitylation, Lys-48-linked polyubiquitylation, or Lys-63-linked polyubiquitylation. Lys-48-linked polyubiquitylation has been studied most and it essentially directs the substrate to degradation by the proteasome. In contrast, the Lys-63-linked polyubiquitylation and monoubiquitylation serve as a signal other than proteasomal-proteolysis (22–24). We first used methylated ubiquitin (hereafter referred to as Met-Ub) in which all lysine residues are blocked by methylation and is incapable of polyubiquitylation. If Parkin catalyzes polyubiquitylation, the use of Met-Ub would shorten the ladder of ubiquitylation but if not, the ubiquitylation pattern would remain unchanged. Unexpectedly, the use of Met-Ub and Uev1-Ubc13 did not change the ubiquitylation pattern, indicating that Parkin catalyzes multiple monoubiquitylation *in vitro* (Fig. 3A). The same result was observed when Ubc7 was used as E2 (Fig. 3B), and these results were more evident when IBR-RING2 (Fig. 4A) was utilized (Fig. 3, C and D). Repeated experiments using lysine-less ubiquitin, in which all lysine residues were changed to arginine, showed it cannot form a polyubiquitin chain, again confirmed the consequence (Fig. 3E). It is noteworthy that sole Ubc13 itself assisted autoubiquitylation of Parkin as well as the Uev1-Ubc13 complex (supplemental Fig. 1B), again supporting this conclusion. These results allowed us to conclude that the mode of ubiquitylation catalyzed by intrinsic Parkin *in vitro* is multiple monoubiquitylation rather than polyubiquitylation (see “Discussion”).

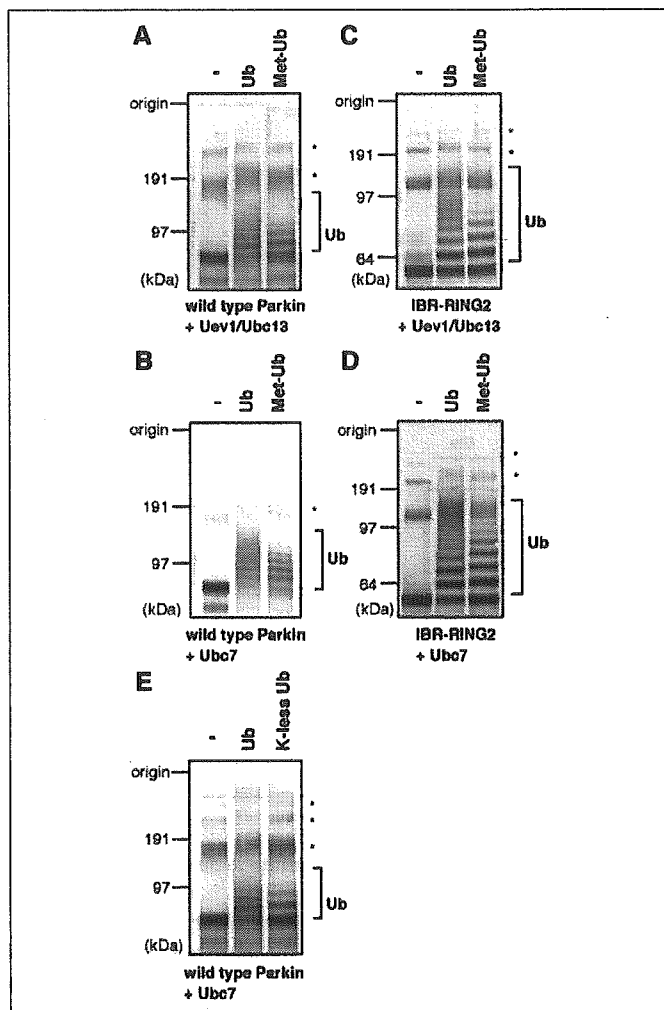


**FIGURE 3. Parkin catalyzes multiple monoubiquitylation.** *A* and *B*, *in vitro* ubiquitylation assay was performed in the absence (–) or presence of ubiquitin (*Ub*) or methylated-ubiquitin (*Met-Ub*; cannot form polyubiquitylation chain). Uev1-Ubc13 was used as E2 in *A* and Ubc7 in *B*. Almost identical ubiquitylation patterns were observed in *Ub* and *Met-Ub*, indicating that Parkin catalyzes multiple monoubiquitylation. *C* and *D*, the result was more evident when IBR-RING2 (see Fig. 4) was utilized. Uev1-Ubc13 was used as E2 in *C* and Ubc7 in *D*. *E*, the same experiment was performed using lysine-less ubiquitin. *Ub*, autoubiquitylation; \*, oligomerization bands. Anti-MBP antibody was used in all experiments.

**Mode of E3 Activity of Parkin with Pathogenic Missense Mutations—**At present, dozens of disease-relevant mutations of Parkin have been reported, and the primary cause of autosomal recessive juvenile parkinsonism is assumed to be impairment of the E3 activity of Parkin by such mutations. However, it is still contentious whether Parkin with PD-causing mutation loses its E3 activity or not (see supplemental Table 1), primarily because of the absence of a sensitive E3-activity assay system using recombinant Parkin. To settle this problem, we examined the E3 activity of MBP-Parkin harboring various mutations and deletions. Three in-frame exonic deletions and 19 PD-linked mutations distributed throughout Parkin were selected (Fig. 4*A*). In addition, two Parkin species, one lacks its Ubl domain ( $\Delta$ Ubl) and the other possesses only C-terminally IBR-RING2 domain (IBR-RING2), were also generated. When these MBP-Parkin mutants were incubated with Ubc7 as E2, only mutations neighboring the second RING finger motif (Fig. 4*A*, *solid circles*) abolished the E3 activity completely (Fig. 4*B*). A nonsense mutation lacking the rear RING finger motif had no E3 activity and sole IBR-RING2 retained the E3 activity (Fig. 4, *light gray circles*), indicating

that the second RING finger motif is the catalytic core for the E3 activity of Parkin. Contrary to what was assumed, all disease-relevant mutations other than those in RING2 still possessed E3 activities equivalent to that of the wild-type Parkin (Fig. 4*B*). The same results were observed when UbcH7 or Uev1-Ubc13 was used as E2 (data not shown). In these assays, we used a bacterially expressed recombinant Parkin, and to our knowledge, this is the first direct evidence that E3 activity of the strictly pure Parkin harboring various pathogenic mutations is not compromised.

## DISCUSSION

To date, numerous biochemical studies have been performed to understand the E3 activity of Parkin. However, it is difficult to rule out the possible involvement of other E3s (see Introduction). Furthermore, the lack of a good model substrate spurs the difficulty to check the intrinsic E3 activity of Parkin. We thus set up a sensitive E3 assay system using bacterially expressed recombinant Parkin. Our assay system has some advantages; namely, we can obtain a large quantity of MBP-Parkin with higher E3 activity than GST-Parkin (Fig. 1). In addition, this fusion protein was already primed for ubiquitylation even in the absence of model substrate, because fused MBP can work as a good pseudo-substrate (Fig. 2). More importantly, because MBP-Parkin is purified from *E. coli*, it is free from possible contamination of other E3(s). The establishment of this assay allowed us to perform a thorough biochemical characterization of Parkin protein.

Interestingly, sole Parkin catalyzes multiple monoubiquitylation *in vitro* (Fig. 3). Moreover, although Doss-Pepe *et al.* (20) reported that Parkin accelerates polyubiquitin chain formation, the MBP-Parkin in our assay did not stimulate the assembly of polyubiquitin chain (Fig. 1*D*, compare lanes 4 and 6, and 10 and 12, respectively). These results seemingly suggest that the ubiquitylation catalyzed by Parkin functions not for proteasomal degradation but for non-proteasomal-proteolytic function(s), such as transcriptional regulation and/or membrane trafficking *in vivo*. However, it is still premature to make such conclusion. Although we showed that pure Parkin catalyzes multiple monoubiquitylation *in vitro* (Fig. 3), some additional factor(s) like E4 can work together *in vivo*, and this needs to be considered. E4 can extend the ubiquitin chain by recognizing the ubiquitin moiety of a ubiquitylated-protein as a substrate (25). If such an E4-like factor(s) cooperates with Parkin *in vivo*, it is still possible that monoubiquitylation catalyzed by Parkin is used as the scaffold for further polyubiquitylation and finally functions for proteasomal degradation. All things considered, further studies are obviously required; in particular, the authentic substrate and the function of Parkin-catalyzed ubiquitylation need to be addressed.

Another unexpected result was that most of the PD-relevant missense mutations do not abrogate E3 activity of Parkin (Fig. 4). Only missense mutations in the rear RING finger motif abolished the E3 activity, revealing that not the first but the second RING finger motif is the catalytic core of Parkin. Recently, several studies that focused on the pathophysiological mechanisms of Parkin have been published (26–30). Although our results on enzymatic activities of mutant Parkin are not fully consistent with previous reports (see supplemental Table 1), methodological differences in the E3 assay may account for the conflicting observation. For example, in one study immunoprecipitated Parkin was used as the source of E3 *in vitro* (31) and in other studies, E3 activity of Parkin was checked by whether or not coexpression of Parkin in cells enhances the ubiquitylation of the putative substrate (7, 30). Although there is little discrepancy, recent studies and our present work drew the same conclusion that the dysfunction of Parkin is not simply attributable to catalytic impairment of its E3 activity. Indeed, several missense mutations cause Parkin to be sequestered into an aggresome-like structure, and this phenomenon may be involved in disease pathogenesis

## Parkin Catalyzes Multiple Monoubiquitylation in Vitro

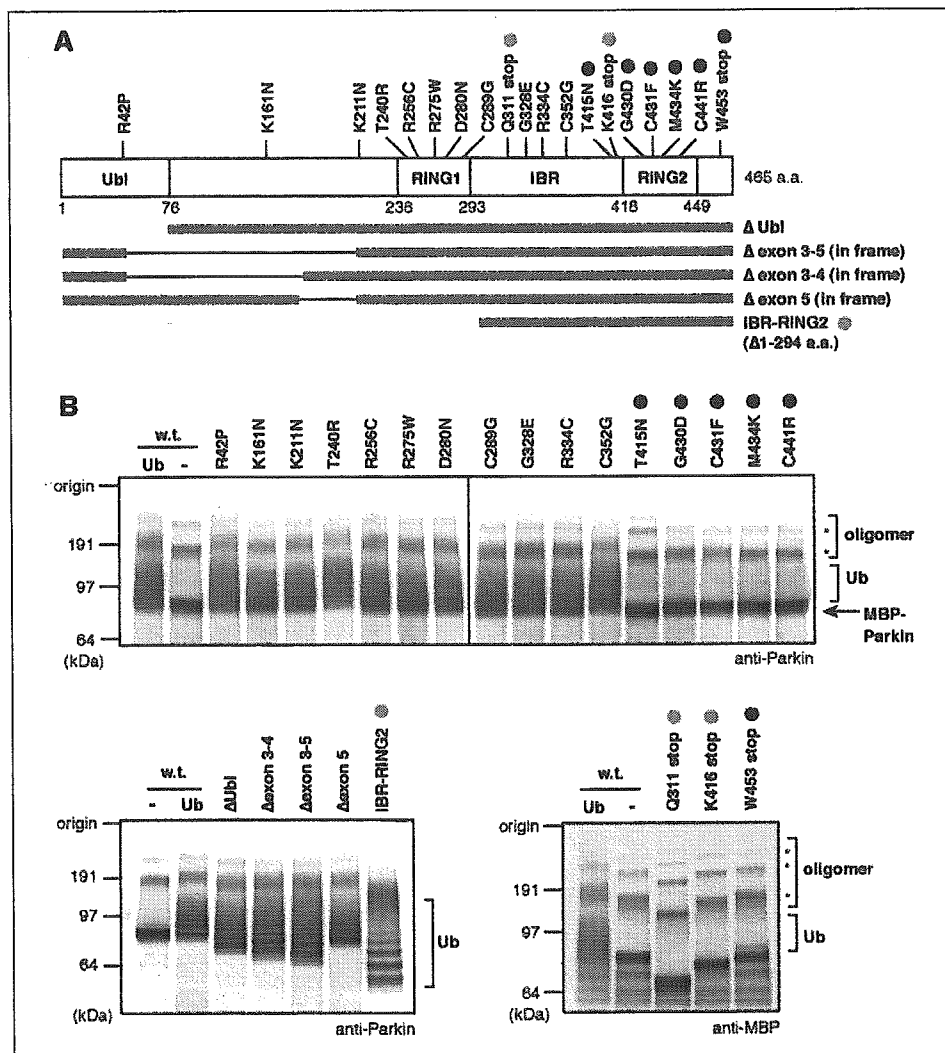


FIGURE 4. *A*, schematic diagram of disease-relevant mutations and exonic deletions of Parkin. *B*, E3 activities of various Parkin proteins bearing PD-linked mutations and deletions. Note that mutations neighboring the second RING finger motif (solid circles) abolished E3 activity of Parkin. Light gray circles indicate that the RING2 is the catalytic core of Parkin (see text for details). Conversely, pathogenic mutants other than RING2 mutants retain E3 activities equivalent to that of the wild-type (w.t.) control. Ub, autoubiquitylation; \*, oligomerization bands.

(27–30). We think that disease-relevant mutations cause not only attenuation of E3 activity but also a variety of primary defects such as sequestration into aggregates and dissociation from its partner protein, and possibly a complex of such defects may eventually lead to Parkin dysfunction and autosomal recessive juvenile parkinsonism.

PD is the second most prevalent neurodegenerative disorder, and thus, analysis of Parkin is important in terms of public welfare. Indeed, a large number of articles on Parkin have been published; however, because of fierce scientific competition, not all Parkin-related phenomena were critically scrutinized although there remains room for close examination. For example, Pawlyk *et al.* (32) recently inspected the anti-Parkin antibodies and uncovered a high non-specificity of the available Parkin antibodies. This also holds true for the E3 activity of Parkin, because precedent works could not exclude the possible involvement of another E3(s). Herein we investigated thoroughly the enzymatic activity of bacterially expressed recombinant Parkin. Although our work is not conspicuous, we hope that our biochemical characterization using pure Parkin would be a solid cornerstone for further studies, as the preceding works were.

**Acknowledgments**—We thank Dr. Tsunehiro Mizushima of Nagoya University for providing recombinant Ubc7 protein. We also thank all members of Prof. K. Tanaka laboratory for the helpful discussions.

## REFERENCES

- Moore, D. J., West, A. B., Dawson, V. L., and Dawson, T. M. (2005) *Annu. Rev. Neurosci.* **28**, 57–87
- Giasson, B. I., and Lee, V. M. (2003) *Cell* **114**, 1–8
- Ross, C. A., and Pickart, C. M. (2004) *Trends Cell Biol.* **14**, 703–711
- Tanaka, K., Suzuki, T., Hattori, N., and Mizuno, Y. (2004) *Biochim. Biophys. Acta* **1695**, 235–247
- Hattori, N., and Mizuno, Y. (2004) *Lancet* **364**, 722–724
- Lohmann, E., Periquet, M., Bonifati, V., Wood, N. W., De Michele, G., Bonnet, A. M., Fraix, V., Broussolle, E., Horstink, M. W., Vidailhet, M., Verpillat, P., Gasser, T., Nicholl, D., Teive, H., Raskin, S., Rascol, O., Destee, A., Ruberg, M., Gasparini, F., Meo, G., Agid, Y., Durr, A., and Brice, A. (2003) *Ann. Neurol.* **54**, 176–185
- Ren, Y., Zhao, J., and Feng, J. (2003) *J. Neurosci.* **23**, 3316–3324
- Corti, O., Hampe, C., Koutnikova, H., Darios, F., Jacquier, S., Prigent, A., Robinson, J. C., Pradier, L., Ruberg, M., Mirande, M., Hirsch, E., Rooney, T., Fournier, A., and Brice, A. (2003) *Hum. Mol. Genet.* **12**, 1427–1437
- Imai, Y., Soda, M., Hatakeyama, S., Akagi, T., Hashikawa, T., Nakayama, K. I., and Takahashi, R. (2002) *Mol. Cell* **10**, 55–67
- Zhong, L., Tan, Y., Zhou, A., Yu, Q., and Zhou, J. (2005) *J. Biol. Chem.* **280**, 9425–9430
- You, J., Cohen, R. E., and Pickart, C. M. (1999) *BioTechniques* **27**, 950–954
- Matsuda, N., Suzuki, T., Tanaka, K., and Nakano, A. (2001) *J. Cell Sci.* **114**, 1949–1957
- Imai, N., Matsuda, N., Tanaka, K., Nakano, A., Matsumoto, S., and Kang, W. (2003) *J. Virol.* **77**, 923–930
- Matsuda, N., Azuma, K., Saijo, M., Iemura, S., Hioki, Y., Natsume, T., Chiba, T., Tanaka, K., and Tanaka, K. (2005) *DNA Repair (Amst.)* **4**, 537–545
- Shimura, H., Hattori, N., Kubo, S., Yoshikawa, M., Kitada, T., Matsumine, H., Asakawa, S., Minoshima, S., Yamamura, Y., Shimizu, N., and Mizuno, Y. (1999) *Ann.*

## Parkin Catalyzes Multiple Monoubiquitylation *In Vitro*

- Neurol.* **45**, 668–672
16. Rankin, C. A., Joazeiro, C. A., Floor, E., and Hunter, T. (2001) *J. Biomed. Sci.* **8**, 421–429
  17. Araki, K., Kawamura, M., Suzuki, T., Matsuda, N., Kanbe, D., Ishii, K., Ichikawa, T., Kumanishi, T., Chiba, T., Tanaka, K., and Nawa, H. (2003) *J. Neurochem.* **86**, 749–762
  18. Takai, R., Matsuda, N., Nakano, A., Hasegawa, K., Akimoto, C., Shibuya, N., and Minami, E. (2002) *Plant J.* **30**, 447–455
  19. Hofmann, R. M., and Pickart, C. M. (1999) *Cell* **96**, 645–653
  20. Doss-Pepe, E. W., Chen, L., and Madura, K. (2005) *J. Biol. Chem.* **280**, 16619–16624
  21. Lim, K. L., Chew, K. C., Tan, J. M., Wang, C., Chung, K. K., Zhang, Y., Tanaka, Y., Smith, W., Engelender, S., Ross, C. A., Dawson, V. L., and Dawson, T. M. (2005) *J. Neurosci.* **25**, 2002–2009
  22. Chen, Z. J. (2005) *Nat. Cell Biol.* **7**, 758–765
  23. Hicke, L. (2001) *Nat. Rev. Mol. Cell Biol.* **2**, 195–201
  24. Pickart, C. M. (2000) *Trends Biochem. Sci.* **25**, 544–548
  25. Richly, H., Rape, M., Braun, S., Rumpf, S., Hoegge, C., and Jentsch, S. (2005) *Cell* **120**, 73–84
  26. Cookson, M. R., Lockhart, P. J., McLendon, C., O'Farrell, C., Schlossmacher, M., and Farrer, M. J. (2003) *Hum. Mol. Genet.* **12**, 2957–2965
  27. Gu, W. J., Corti, O., Araujo, F., Hampe, C., Jacquier, S., Lucking, C. B., Abbas, N., Duyckaerts, C., Rooney, T., Pradier, L., Ruberg, M., and Brice, A. (2003) *Neurobiol. Dis.* **14**, 357–364
  28. Henn, I. H., Gostner, J. M., Lackner, P., Tatzelt, J., and Winklhofer, K. F. (2005) *J. Neurochem.* **92**, 114–122
  29. Wang, C., Tan, J. M., Ho, M. W., Zaiden, N., Wong, S. H., Chew, C. L., Eng, P. W., Lim, T. M., Dawson, T. M., and Lim, K. L. (2005) *J. Neurochem.* **93**, 422–431
  30. Sriram, S. R., Li, X., Ko, H. S., Chung, K. K., Wong, E., Lim, K. L., Dawson, V. L., and Dawson, T. M. (2005) *Hum. Mol. Genet.* **14**, 2571–2586
  31. Staropoli, J. F., McDermott, C., Martinat, C., Schulman, B., Demireva, E., and Abeliovich, A. (2003) *Neuron* **37**, 735–749
  32. Pawlyk, A. C., Giasson, B. I., Sampathu, D. M., Perez, F. A., Lim, K. L., Dawson, V. L., Dawson, T. M., Palmiter, R. D., Trojanowski, J. Q., and Lee, V. M. (2003) *J. Biol. Chem.* **278**, 48120–48128



## COMMUNICATION

# The Crystal Structure of Human Atg4b, a Processing and De-conjugating Enzyme for Autophagosome-forming Modifiers

Taichi Kumanomidou<sup>1</sup>, Tsunehiro Mizushima<sup>1,2</sup>, Masaaki Komatsu<sup>3,4</sup>,  
Atsuo Suzuki<sup>1</sup>, Isei Tanida<sup>4</sup>, Yu-shin Sou<sup>4</sup>, Takashi Ueno<sup>4</sup>,  
Eiki Kominami<sup>4</sup>, Keiji Tanaka<sup>3\*</sup> and Takashi Yamane<sup>1\*</sup>

<sup>1</sup>Department of Biotechnology  
Graduate School of Engineering  
Nagoya University, Chikusa-ku  
Nagoya 464-8603, Japan

<sup>2</sup>PRESTO, Japan Science and  
Technology Agency, Kawaguchi  
Saitama 332-0012, Japan

<sup>3</sup>Laboratory of Frontier Science  
Tokyo Metropolitan Institute of  
Medical Science, Bunkyo-ku  
Tokyo 113-8613, Japan

<sup>4</sup>Department of Biochemistry  
Juntendo University School of  
Medicine, Bunkyo-ku, Tokyo  
113-8421, Japan

Autophagy is an evolutionarily conserved pathway in which the cytoplasm and organelles are engulfed within double-membrane vesicles, termed autophagosomes, for the turnover and recycling of these cellular constituents. The yeast Atg8 and its human orthologs, such as LC3 and GABARAP, have a unique feature as they conjugate covalently to phospholipids, differing from ubiquitin and other ubiquitin-like modifiers that attach only to protein substrates. The lipidated Atg8 and LC3 localize to autophagosomal membranes and play indispensable roles for maturation of autophagosomes. Upon completion of autophagosome formation, some populations of lipidated Atg8 and LC3 are delipidated for recycling. Atg4b, a specific protease for LC3 and GABARAP, catalyzes the processing reaction of LC3 and GABARAP precursors to mature forms and de-conjugating reaction of the modifiers from phospholipids. Atg4b is a unique enzyme whose primary structure differs from that of any other proteases that function as processing and/or de-conjugating enzymes of ubiquitin and ubiquitin-like modifiers. However, the tertiary structures of the substrates considerably resemble that of ubiquitin except for the N-terminal additional domain. Here we determined the crystal structure of human Atg4b by X-ray crystallography at 2.0 Å resolution, and show that Atg4b is a cysteine protease whose active catalytic triad site consists of Cys74, His280 and Asp278. The structure is comprised of a left lobe and a small right lobe, designated the “protease domain” and the “auxiliary domain”, respectively. Whereas the protease domain structure of Atg4b matches that of papain superfamily cysteine proteinases, the auxiliary domain contains a unique structure with yet-unknown function. We propose that the R229 and W142 residues in Atg4b are specifically essential for recognition of substrates and catalysis of both precursor processing and de-conjugation of phospholipids.

© 2005 Elsevier Ltd. All rights reserved.

**Keywords:** Atg4b; autophagy; ubiquitin-like modifier; cysteine protease; tertiary structure

\*Corresponding authors

There is growing evidence regarding the importance of ubiquitin (Ub) and ubiquitin-like proteins

Abbreviations used: Ub, ubiquitin; Ubl, ubiquitin-like protein; GABARAP, gamma-aminobutyric-acid type-A receptor-associated protein; PE, phosphatidylethanolamine.

E-mail addresses of the corresponding authors:  
tanakak@rinshoken.or.jp; yamane@nubio.nagoya-u.ac.jp

(Ubls) as landmark molecules of new type post-translational protein-modifying systems responsible for diverse cellular activities, such as intracellular protein proteolysis and other non-proteolytic roles in eukaryotic cells.<sup>1–3</sup> Ub and Ubls are covalently attached to client molecules by an elaborate cascade system consisting of activating (E1), conjugating (E2), and/or ligating (E3) enzymes. Intriguingly, Ub is encoded by two types

of unique genes; a poly(Ub) gene, which encodes a tandemly repeated Ub (so-called "heat-shock gene"), and an Ub-fused gene with certain ribosomal proteins of unknown biological significance.<sup>4,5</sup> In addition, some Ubl modifiers (if not all) are also synthesized in precursor forms with extension adducts (consisting of several amino acid residues) in the COOH-termini. The Ub-fused proteins and the extra adducts of Ubls must be cleaved prior to their conjugation to target molecules. It is noteworthy that most of these Ub and Ubl-modifying reactions are reversible; i.e. Ub/Ubl-conjugates are de-conjugated from the substrates to abolish the effects of modifications, and then the Ub/Ubl modifiers are re-utilized for other cycles of respective modifications.<sup>6</sup> For these events, various enzymes catalyze the maturation of precursor modifiers (i.e. reactions that produce functional Ub or Ubl moieties from their precursor forms) and de-conjugation of Ub or Ubl-ligated molecules in eukaryotic cells. These enzymes belong to a large protein family of cysteine proteases, with the exception of certain de-ubiquitinating enzymes that are metalloproteases.<sup>7</sup>

Human Atg4b, the yeast Atg4 homologue essential for autophagy, cleaves the COOH-terminal adducts of microtubule-associated protein 1 light chain 3 (LC3) and gamma-aminobutyric-acid type-A receptor-associated protein (GABARAP), a human Atg8 ortholog.<sup>8,9</sup> Among the Ubl modifiers, the yeast Atg8 and its human orthologs have a unique feature in that they conjugate covalently to phospholipids such as phosphatidylethanolamine (PE), thus differing from any other ubiquitin-like modifiers that conjugate only to protein substrates.<sup>8-10</sup> In this regard, the Atg8/LC3 conjugation system to phospholipids is essential for autophagy, a membrane trafficking mechanism that delivers cytoplasmic constituents into the lysosome/vacuole for bulk protein degradation.<sup>11,12</sup> The initial step of autophagy is elongation of the isolation membrane. The isolation membrane envelops cytoplasmic components including organelles, and then its edges fuse with each other forming a double membrane structure called autophagosome. Finally, the outer membrane of the autophagosome fuses to the lysosome/vacuole and the sequestered cytoplasmic constituents are degraded by the lysosomal/vacuolar hydrolases, together with the inner membrane of the autophagosomes.<sup>13</sup> In this process, the processing of LC3 by Atg4b is essential for LC3-lipidation during autophagosome formation. Lipidated LC3 localizes to autophagosomes and some populations are delipidated by Atg4b after autophagosome maturation for recycling.<sup>9,14</sup> Considering the specific function of Atg8/LC3 family proteins, it is necessary to determine the structure of this processing/de-conjugating enzyme, Atg4b. Here we report for the first time the tertiary structure and the substrate recognition mechanism of Atg4b and compare these properties to those of other de-ubiquitylating enzymes and structurally similar proteases.

## Overall structure of Atg4b

The structure determination process is summarized in Table 1. Atg4b adapts an  $\alpha/\beta$  structure with overall dimensions of 60 Å × 55 Å × 50 Å consisting of 13  $\beta$ -strands designated  $\beta$ 1– $\beta$ 13, eight  $\alpha$ -helices ( $\alpha$ 1– $\alpha$ 8) and three  $3_{10}$  helices. The  $3_{10}$ -1 helix is located at the N-terminal region,  $3_{10}$ -2 is in the loop between  $\beta$ 10 and  $\beta$ 11, and  $3_{10}$ -3 is in between  $\beta$ 11 and  $\beta$ 12. Atg4b is composed of a left lobe and a small right lobe, designated the "protease domain" and the "auxiliary domain", respectively (Figure 1(a)). The structure from residues 191 to 215, which links the auxiliary domain and protease domain, could not be constructed because of the weak electron density. Despite the lack of obvious sequence homology to papain, the protease domain of Atg4b matches that of papain superfamily cysteine proteases. Superposition of Atg4b with papain on the 119 C $\alpha$  atoms of the optimal Atg4b–papain overlap resulted in a root-mean-square deviation (r.m.s.d.) of 2.1 Å (Figure 1(b)). The secondary structure elements of the central antiparallel  $\beta$ -sheet ( $\beta$ 11,  $\beta$ 9,  $\beta$ 8,  $\beta$ 7,  $\beta$ 12 and  $\beta$ 6) and helix  $\alpha$ 2 are structurally equivalent to those of papain-like proteases (Figure 1(c)). The protease domain of Atg4b is divided into two distinct sub-domains and the active site of Atg4b is located between the two sub-domains (Figure 1(a) and (c)). On the other hand, the auxiliary domain contains two  $\beta$ -strands and two  $\alpha$ -helices, in which the papain superfamily does not hold (Figure 1(b)). The auxiliary domain may provide additional functions, such as substrate recognition.

The structure of Atg4b was compared with those of other proteins in the PDB database using the DALI server.<sup>15</sup> Atg4b is structurally similar to a cysteine protease, IdeS (PDB ID code 1y08),<sup>16</sup> with a r.m.s.d. value of 3.8 Å. IdeS is also an endopeptidase with uniquely high specificity. This protease recognizes the L-L-G-G motif in IgG. Comparison of the primary structures of Atg4b and IdeS showed an homology of approximately 20%.

## Mechanism of catalysis

A decrease in enzymatic activity after mutation of residues H280 and D278 indicates that these amino acid residues form a catalytic triad (data not shown). The active site cysteine, C74, histidine and aspartate residues are well conserved in all known Atg4 sequences.<sup>17</sup> The active site of Atg4b is located at the N-terminal region of helix  $\alpha$ 2 and the loop connecting strands  $\beta$ 9 and  $\beta$ 10. The active site of Atg4b fits the corresponding residues in UCH-L3,<sup>18</sup> papain,<sup>19</sup> cathepsin B,<sup>20</sup> and HAUSP<sup>21</sup> (Figure 2(a)). The hydrogen bond network between Atg4b and others is essentially the same. However, the orientation of the imidazole ring of H280 of Atg4b is clearly different from those of other cysteine proteases. The C $\alpha$  position of H280 in Atg4b is located on the opposite side of the active site H159 in papain.<sup>19</sup> The structural similarity at

**Table 1.** Data collection, phasing and refinement statistics

	Native 1	Native 2	Thimerosal	Hg (CH <sub>3</sub> COO) <sub>2</sub>	Pb (CH <sub>3</sub> COO) <sub>2</sub>	IrCl <sub>3</sub>	K <sub>2</sub> PtCl <sub>6</sub>
<i>A. Data collection</i>							
Space group	<i>P</i> 2 <sub>1</sub>	<i>P</i> 2 <sub>1</sub>	–	–	–	–	–
Resolution (Å)	2.0	2.0	2.4	3.3	2.4	2.6	2.8
Observations	180,458	114,063	122,583	40,417	86,164	76,675	40,579
Unique reflections	48,166	39,483	27,747	10,816	24,628	20,857	16,168
Completeness (%) (last shell)	98.7 (99.1)	81.5 (73.2)	98.5 (98.6)	99.8 (100.0)	88.6 (81.6)	95.0 (100.0)	92.4 (96.1)
Redundancy	3.7 (3.3)	2.9 (2.4)	4.4 (4.1)	3.7 (3.8)	3.6 (3.3)	3.7 (3.8)	2.5 (2.5)
<i>R</i> <sub>sym</sub> (%) (last shell)	3.0 (16.3)	3.7 (30.7)	5.6 (19.3)	7.0 (27.6)	3.9 (28.6)	3.9 (19.9)	5.8 (28.0)
<i>I</i> / $\sigma$	23.8	19.5	16.6	12.2	17.8	18.2	12.6
<i>B. MIRAS phasing</i>							
Resolution (Å)	–	–	2.4	3.3	2.4	2.6	2.8
<i>R</i> <sub>iso</sub> versus Native 2	–	–	0.199	0.195	0.155	0.106	0.108
Heavy atom sites	–	–	9	3	4	4	3
Phasing power (anomalous)	–	–	1.486 (1.055)	0.016 (0.008)	0.062 (0.032)	0.079 (0.035)	0.022 (0.009)
<i>R</i> <sub>cullis</sub> (anomalous)	–	–	0.608 (0.803)	0.835 (0.912)	0.699 (0.959)	0.603 (0.945)	0.867 (1.000)
<i>C. Refinement statistics</i>							
Resolution range (Å)	45.0–2.00	–	–	–	–	–	–
Reflections	45,690	–	–	–	–	–	–
Protein atoms	5386	–	–	–	–	–	–
Solvent	337	–	–	–	–	–	–
<i>R</i> <sub>cryst</sub> / <i>R</i> <sub>free</sub> (%)	22.0/28.3	–	–	–	–	–	–
<i>D. r.m.s.d. from ideal values</i>							
Bond length (Å)	0.011	–	–	–	–	–	–
Bond angle (deg.)	1.42	–	–	–	–	–	–
<i>Ramachandran plot</i>							
Most favored (%)	87.6	–	–	–	–	–	–
Additionally allowed (%)	10.3	–	–	–	–	–	–
Generously allowed (%)	2.1	–	–	–	–	–	–

The full-length human Atg4b was cloned into pGEX-6P (Amersham Biosciences). For overexpression in *E. coli*, the recombinant plasmid was transformed into BL21 (RIL) (Novagen). Protein expression was induced at 35.5 °C with 0.1 mM isopropyl- $\beta$ -D-thiogalactoside. After further growth for 4 h, the bacteria were pelleted, resuspended in 20 mM Tris-HCl (pH 7.4) and 150 mM NaCl, and lysed by sonication. The resulting soluble fraction was purified using glutathione Sepharose 4B and anion exchange chromatography. The GST moiety was proteolytically removed by PreScission protease. Crystals of Atg4b were obtained at 15 °C by the hanging-drop vapor-diffusion method, with a mixture of 2.0  $\mu$ l of protein (6.8 mg/ml) in buffer containing 25 mM Tris-HCl (pH 7.5), 1 mM dithiothreitol (DTT), and the same volume of reservoir solution (0.65–0.70 M sodium citrate (pH 6.5)). The crystals belong to the space group *P*2<sub>1</sub>, with *a* = 51.28 Å, *b* = 161.32 Å, *c* = 51.27 Å, and  $\beta$  = 119.6°. There are two molecules per asymmetric unit. The crystals were equilibrated in a cryo-protectant buffer containing reservoir buffer plus 10%(v/v) glycerol and then frozen in a cold nitrogen stream at 100 K. Heavy-atom soaks were performed in crystallization buffer with 0.01 mM thimerosal (22 h), 0.01 mM Hg(CH<sub>3</sub>COO)<sub>2</sub> (7 min), Pb(CH<sub>3</sub>COO)<sub>2</sub> (22 h), IrCl<sub>3</sub> (18 h) and K<sub>2</sub>PtCl<sub>6</sub> (22 h). All data sets were collected on beamline BL44XU at Spring-8, and processed using the software Denzo and ScaLpack and programs from CCP4 package. The structure of Atg4b was determined using Native 2 dataset by the multiple isomorphous replacement anomalous scattering (MIRAS) method. Atomic positions for heavy-atoms in the asymmetric unit were determined by using SHELXD<sup>26</sup> and refined by using SHARP. Initial MIRAS phases were extended to 2.0 Å and improved with solvent flattening and histogram matching using DM. The initial model was constructed with the program ARP/wARP.<sup>27</sup> Atg4b crystals showed low isomorphism between different native crystals. The final Atg4b structure was determined using Native 2 dataset with high completeness by the molecular replacement technique. As the search model, the initial model was applied. The warpNtrace mode of ARP/wARP then built a model automatically, which had 570 of the 786 amino acid residues of Atg4b in the native electron density at a resolution of 2.0 Å. The remaining parts of the structure were built manually using the program XtalView.<sup>28</sup> The model was refined at 2.0 Å resolution using the program REFMAC5.<sup>29</sup> The final refined model contained two molecules. Both models contained residues 10–190 and 216–373. The Table lists the methods used for data collection and phasing and refinement statistics. Data for the outer shell are in parentheses.

the active sites suggests that the catalytic mechanism of Atg4b is similar to that of papain. In Atg4b, C74 and H280 form a thiolate imidazolium ion pair, and D278 functions to orient the active site residues correctly and stabilizes the protonated form of H280, while Y54 plays a role in the oxyanion hole. Comparison of the surface representations of both enzymes revealed that both active site clefts are formed between two distinct sub-domains (Figure 2(b)). While the active site cleft of papain is open and allows accessing the substrate, the corresponding active site cleft of Atg4b is closed by

lid loop of the enzyme. The lid loop (residues 258–263, especially N261) connecting  $\beta$ 7 and  $\beta$ 8 covers the active site C74 though it is flexible because of the residues' high temperature factors (Figure 3(a) and (b)). Indeed, the hydrogen bond network between N261 and the active site residue is observed *via* a water molecule (Figure 3(b)). The scheme of the hydrogen bonds is N261···Wat49, Wat49···C74 and Wat49···Y54. Notably, the space for substrate binding is very small in the active site, suggesting a closed structure, corresponding to a self-inhibited state. This conformation is not likely to be

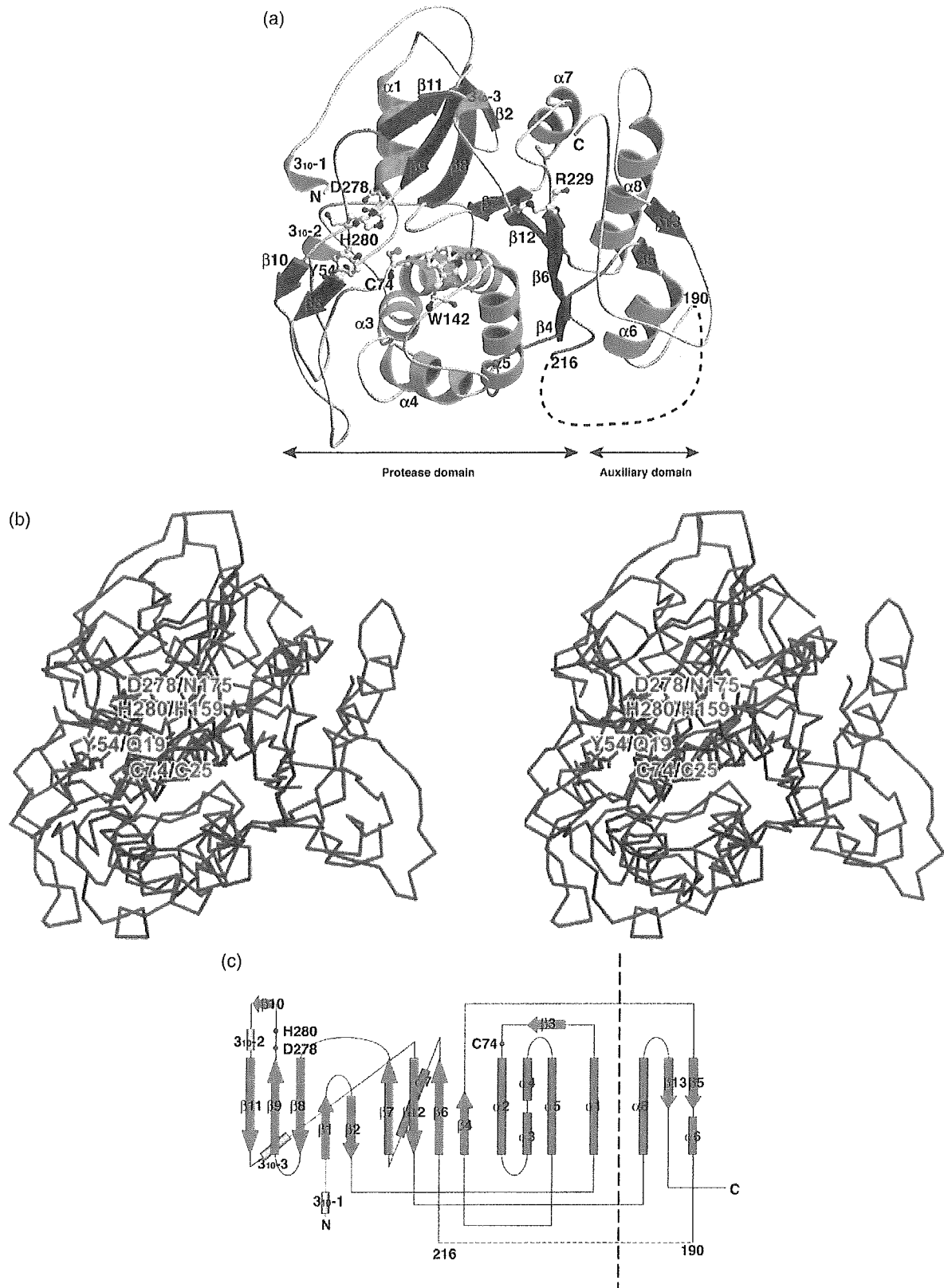


**Figure 1.** (a) Schematic drawing of Atg4b. The color codes for the secondary structure elements are:  $\alpha$ -helix, cyan;  $\beta$ -strands, magenta; loops, salmon. The active site residues Y54, C74, W142, R229, D278 and H280 are shown in ball-and-stick representation. (b) Stereo diagram showing the superposition of  $C^\alpha$  of Atg4b (blue) and papain (red). (For 119 aligned  $C^\alpha$  atoms, r.m.s.d. = 2.1 Å.) (c) A topology diagram of Atg4b. The  $\alpha$ -helices appear as cyan-colored cylinders and are labeled  $\alpha 1$ – $\alpha 8$ . The  $\beta$ -strands appear as magenta-colored arrows and are labeled  $\beta 1$ – $\beta 13$ . The  $3_{10}$  helices appear as gray-colored cylinders and are labeled  $3_{10-1}$ – $3_{10-3}$ . Red circles indicate the positions of the active site residues.



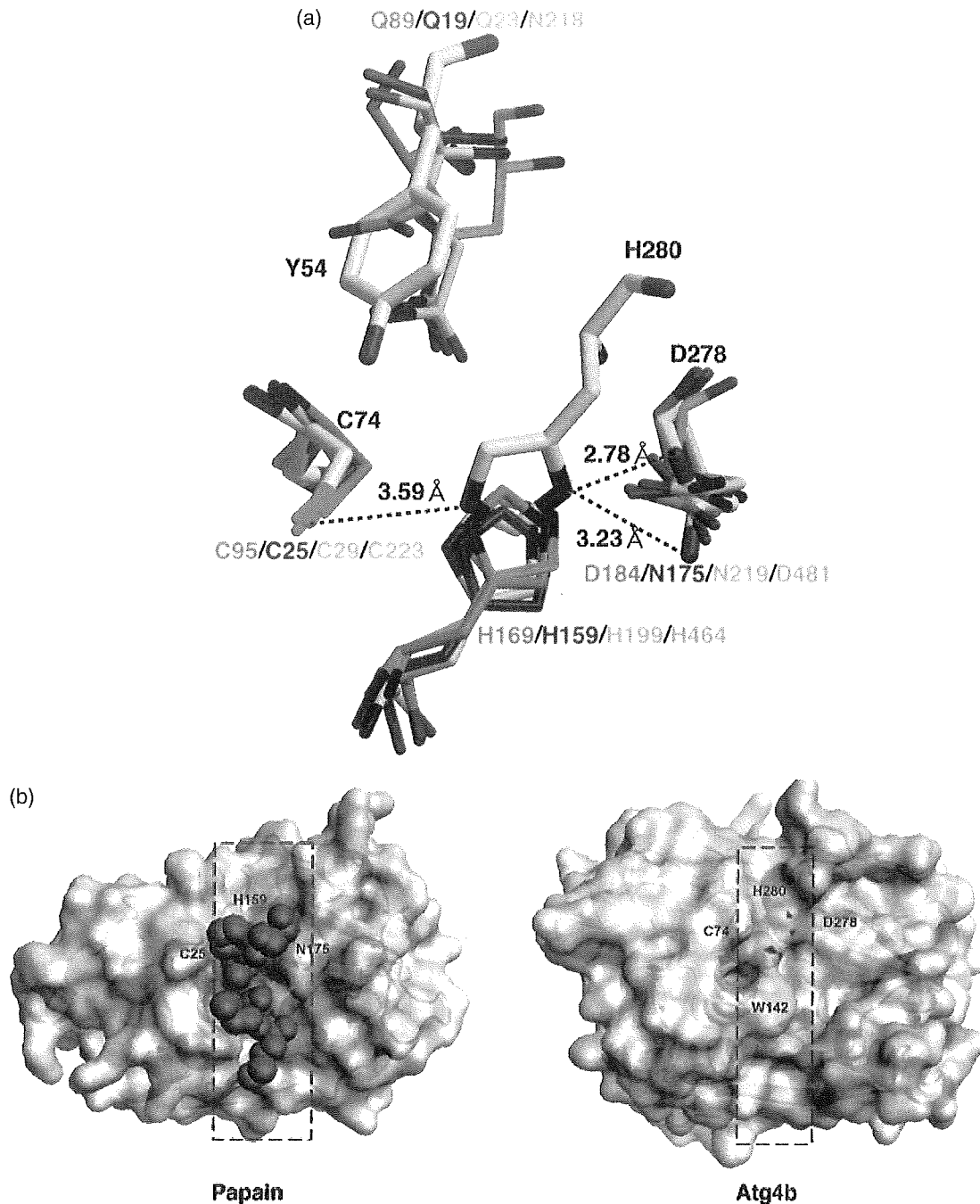


**Figure 2.** Comparison of the active sites among Atg4b and papain-like proteases. Active site residues of Atg4b, Y54, C74, D278 and H280 are shown as yellow stick models. Those of four papain-like cysteine proteases appear in cyan (UCH-L3: PDB ID code 1xd3), magenta (papain: PDB ID code 1pop), gold (cathepsin B: PDB ID code 1ito) and salmon (UBP: PDB ID code 1nbf). The Figure was prepared by superposition of UCH-L3, papain, cathepsin B and UBP on Atg4b. (b) Surface representation of papain complex with the N-terminal region of stefin B (PDB ID code 1stf)<sup>25</sup> and Atg4b. Protein surfaces are colored gray. The wavy line surrounds active site clefts. Bound stefin B is in red. The active site residues are in magenta.

a consequence of crystal packing. It is conceivable that the lid loop undergoes conformational change to an open form upon substrate binding.

### Substrate recognition

Next, we conducted site-directed mutagenesis to change key residues assumed to participate in

catalysis and substrate recognition of Atg4b. To investigate the processing activation of Atg4b against two Atg4b substrates, LC3 and GABARAP, *in vitro*, recombinant Atg4b proteins expressed in *Escherichia coli* were purified to homogeneity. As substrates, the C-terminal Myc-tagged LC3 (LC3-Myc) and GABARAP (GABARAP-Myc) were expressed in *E. coli* and purified to homogeneity.

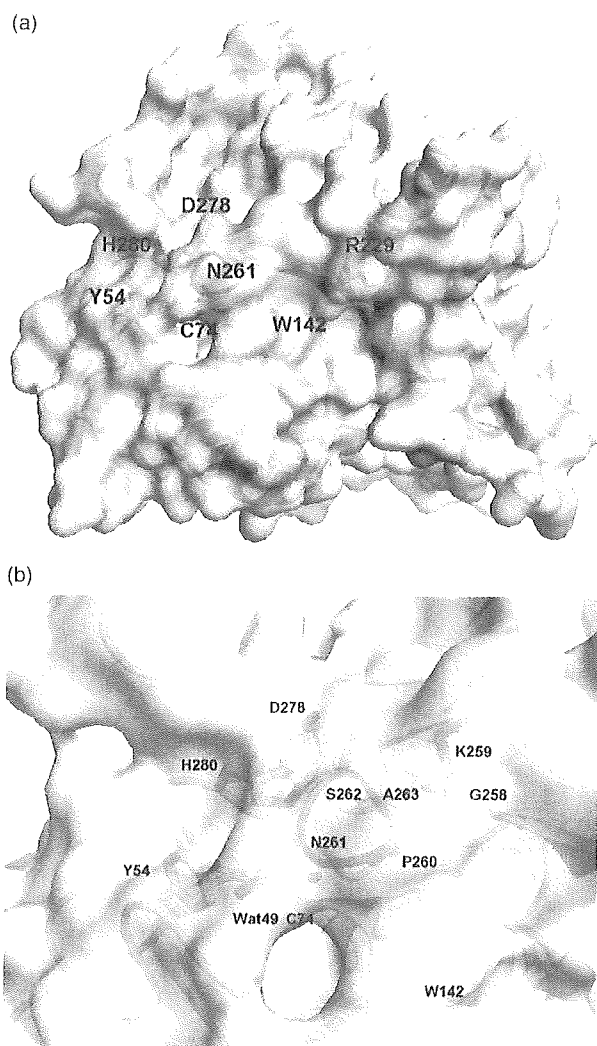


**Figure 3.** (a) Surface representation of Atg4b. The active site and the proposed substrate recognizing residues are individually labeled. (b) Clipping of the active site, Y54, C74, W142, D278 and H280, is shown in ball-and-stick representation. The red sphere is a water molecule. The lid loop (residues 258–263) covers the active site.

Incubation of each substrate with Atg4b released the Myc-tag, resulting in LC3 and GABARAP products, respectively, that migrated firstly in SDS-PAGE. For each mutant of Atg4b, the extent of the cleavage was determined by scanning Coomassie blue-stain (Supplementary Data, Figure S1a). Wild-type Atg4b cleaved both substrates. As expected, mutation of cysteine-74, one of the residues that comprises the catalytic triad was associated with a complete disappearance of the processing activity. Mutation of other residues comprising the catalytic triad also resulted in the loss of activity (data not shown). Since the crystal structures of LC3 and GABARAP were determined,<sup>22,23</sup> we built the model of the LC3 or GABARAP and Atg4b complex manually to predict key residues of Atg4b for substrate recognition. The interactions between the Ubl modifier, NEDD8 and its specific cysteine protease, NEDP1 also provided useful information.<sup>24</sup> Thus, W142 of Atg4b was

predicted to form a  $\pi$ -stacking with F119 of LC3 and Y115 of GABARAP, which immediately precedes Gly. In addition, R229 of Atg4b was predicted to form a hydrogen bond with Q116 of LC3 and a salt-bridge with E112 of GABARAP. These appear to be key interactions, as neither the W142A nor R229A versions of Atg4b showed severe reduction of the protease activity.

While the assay employed the measures described above the processing activity of Atg4b *in vitro* it was also important to assay the de-conjugating activity of the protease. Using our recently developed *in vitro* reconstitution systems (Y.S., I. T., M.K., T.U. & E.K., unpublished results), we generated PE-conjugating LC3 and GABARAP (Supplementary Data, Figure S1b). The modified substrates migrated first compared with the unmodified substrates. Incubation of each substrate with Atg4b released PE, resulting in LC3 and GABARAP products, respectively, which migrated slowly in SDS-PAGE. For each mutant, the extent of cleavage was determined by immunoblotting with anti-LC3 and anti-GABARAP, respectively (Supplementary Data, Figure S1b). When the wild-type Atg4b was mixed with the substrates, both modified substrates were completely delipidated. Mutants with reduced activity, as demonstrated in the processing assay, were also defective in the de-conjugating assay. These results indicate that W142 and R229 residues in Atg4b are essential for recognition of both lipidated and native substrates.

In conclusion, we have demonstrated here that Atg4b is an endopeptidase with a unique high specificity toward Atg8 homologues, such as LC3 and GABARAP. Analysis of the crystal structure of the human Atg4b showed a catalytic mechanism similar to the papain superfamily cysteine proteinases. The mode of interaction between Atg4b and Atg8 homologues may be determined in the future by their co-crystallization.

#### Protein Data Bank accession code

The coordinates and structure factors have been deposited in the RCSB PDB (accession code 2D1I).

#### Acknowledgements

We thank all members of the BL44XU for their help in data collection at SPring-8. This work was supported by Grants-in-Aid for Scientific Research on Priority Area (C) from the Ministry of Education, Culture, Science and Technology of Japan.

#### Supplementary Data

Supplementary data associated with this article can be found, in the online version, at doi:10.1016/j.jmb.2005.11.018

## References

1. Jentsch, S. & Pyrowolakis, G. (2000). Ubiquitin and its kin: how close are the family ties? *Trends Cell Biol.* **10**, 335–342.
2. Pickart, C. M. & Eddins, M. J. (2004). Ubiquitin: structures, functions, mechanisms. *Biochim. Biophys. Acta*, **1695**, 55–72.
3. Welchman, R. L., Gordon, C. & Mayer, R. J. (2005). Ubiquitin and ubiquitin-like proteins as multifunctional signals. *Nature Rev. Mol. Cell Biol.* **6**, 599–609.
4. Finley, D., Bartel, B. & Varshavsky, A. (1989). The tails of ubiquitin precursors are ribosomal proteins whose fusion to ubiquitin facilitates ribosome biogenesis. *Nature*, **338**, 394–401.
5. Wiborg, O., Pedersen, M. S., Wind, A., Berglund, L. E., Marcker, K. A. & Vuust, J. (1985). The human ubiquitin multigene family: some genes contain multiple directly repeated ubiquitin coding sequences. *EMBO J.* **4**, 755–759.
6. Schwartz, D. C. & Hochstrasser, M. (2003). A superfamily of protein tags: ubiquitin, SUMO and related modifiers. *Trends Biochem. Sci.* **28**, 321–328.
7. Kim, J. H., Park, K. C., Chung, S. S., Bang, O. & Chung, C. H. (2003). Deubiquitinating enzymes as cellular regulators. *J. Biochem. (Tokyo)*, **134**, 9–18.
8. Kabeya, Y., Mizushima, N., Yamamoto, A., Oshitani-Okamoto, S., Ohsumi, Y. & Yoshimori, T. (2004). LC3, GABARA and GATE16 localize to autophagosomal membrane depending on form-II formation. *J. Cell Sci.* **117**, 2805–2812.
9. Tanida, I., Sou, Y. S., Ezaki, J., Minematsu-Ikeguchi, N., Ueno, T. & Kominami, E. (2004). HsAtg4B/HsApg4B/autophagin-1 cleaves the carboxyl termini of three human Atg8 homologues and delipidates microtubule-associated protein light chain 3- and GABAA receptor-associated protein-phospholipid conjugates. *J. Biol. Chem.* **279**, 36268–36276.
10. Ichimura, Y., Kirisako, T., Takao, T., Satomi, Y., Shimonishi, Y., Ishihara, N. *et al.* (2000). A ubiquitin-like system mediates protein lipidation. *Nature*, **408**, 488–492.
11. Klionsky, D. J. (2005). The molecular machinery of autophagy: unanswered questions. *J. Cell Sci.* **118**, 7–18.
12. Ohsumi, Y. (2001). Molecular dissection of autophagy: two ubiquitin-like systems. *Nature Rev. Mol. Cell Biol.* **2**, 211–216.
13. Mizushima, N., Ohsumi, Y. & Yoshimori, T. (2002). Autophagosome formation in mammalian cells. *Cell Struct. Funct.* **27**, 421–429.
14. Kabeya, Y., Mizushima, N., Ueno, T., Yamamoto, A., Kirisako, T., Noda, T. *et al.* (2000). LC3, a mammalian homologue of yeast Apg8p, is localized in autophagosome membranes after processing. *EMBO J.* **19**, 5720–5728.
15. Holm, L. & Sander, C. (1993). Protein structure comparison by alignment of distance matrices. *J. Mol. Biol.* **233**, 123–138.
16. Wenig, K., Chatwell, L., von Pawel-Rammingen, U., Bjorck, L., Huber, R. & Sondermann, P. (2004). Structure of the streptococcal endopeptidase IdeS, a cysteine proteinase with strict specificity for IgG. *Proc. Natl Acad. Sci. USA*, **101**, 17371–17376.
17. Kirisako, T., Ichimura, Y., Okada, H., Kabeya, Y., Mizushima, N., Yoshimori, T. *et al.* (2000). The reversible modification regulates the membrane-binding state of Apg8/Aut7 essential for autophagy and the cytoplasm to vacuole targeting pathway. *J. Cell Biol.* **151**, 263–276.
18. Johnston, S. C., Larsen, C. N., Cook, W. J., Wilkinson, K. D. & Hill, C. P. (1997). Crystal structure of a deubiquitinating enzyme (human UCH-L3) at 1.8 Å resolution. *EMBO J.* **16**, 3787–3796.
19. Schroder, E., Phillips, C., Garman, E., Harlos, K. & Crawford, C. (1993). X-ray crystallographic structure of a papain-leupeptin complex. *FEBS Letters*, **315**, 38–42.
20. Yamamoto, A., Tomoo, K., Matsugi, K., Hara, T., In, Y., Murata, M. *et al.* (2002). Structural basis for development of cathepsin B-specific noncovalent-type inhibitor: crystal structure of cathepsin B-E64c complex. *Biochim. Biophys. Acta*, **1597**, 244–251.
21. Hu, M., Li, P., Li, M., Li, W., Yao, T., Wu, J. W. *et al.* (2002). Crystal structure of a UBP-family deubiquitinating enzyme in isolation and in complex with ubiquitin aldehyde. *Cell*, **111**, 1041–1054.
22. Sugawara, K., Suzuki, N. N., Fujioka, Y., Mizushima, N., Ohsumi, Y. & Inagaki, F. (2004). The crystal structure of microtubule-associated protein light chain 3, a mammalian homologue of *Saccharomyces cerevisiae* Atg8. *Genes Cells*, **9**, 611–618.
23. Bavro, V. N., Sola, M., Bracher, A., Kneussel, M., Betz, H. & Weissenhorn, W. (2002). Crystal structure of the GABA(A)-receptor-associated protein, GABARAP. *EMBO Rep.* **3**, 183–189.
24. Shen, L. N., Liu, H., Dong, C., Xirodimas, D., Naismith, J. H. & Hay, R. T. (2005). Structural basis of NEDD8 ubiquitin discrimination by the deNEDDylating enzyme NEDP1. *EMBO J.* **24**, 1341–1351.
25. Stubbs, M. T., Laber, B., Bode, W., Huber, R., Jerala, R., Lenarcic, B. & Turk, V. (1990). The refined 2.4 Å X-ray crystal structure of recombinant human stefin B in complex with the cysteine proteinase papain: a novel type of proteinase inhibitor interaction. *EMBO J.* **9**, 1939–1947.
26. Schneider, T. R. & Sheldrick, G. M. (2002). Substructure solution with SHELXD. *Acta Crystallog. sect. D*, **58**, 1772–1779.
27. Perrakis, A., Morris, R. & Lamzin, V. S. (1999). Automated protein model building combined with iterative structure refinement. *Nature Struct. Biol.* **6**, 458–463.
28. McRee, D. E. (1999). XtalView/Xfit—A versatile program for manipulating atomic coordinates and electron density. *J. Struct. Biol.* **125**, 156–165.
29. Murshudov, G. N., Vagin, A. A., Lebedev, A., Wilson, K. S. & Dodson, E. J. (1999). Efficient anisotropic refinement of macromolecular structures using FFT. *Acta Crystallog. sect. D*, **55**, 247–255.

Edited by K. Morikawa

(Received 13 September 2005; received in revised form 4 November 2005; accepted 6 November 2005)  
Available online 28 November 2005

# Excess Peroxisomes Are Degraded by Autophagic Machinery in Mammals\*

Received for publication, November 15, 2005. Published, JBC Papers in Press, December 6, 2005, DOI 10.1074/jbc.M512283200

Jun-ichi Iwata<sup>‡§1</sup>, Junji Ezaki<sup>‡1</sup>, Masaaki Komatsu<sup>‡§</sup>, Sadaki Yokota<sup>¶</sup>, Takashi Ueno<sup>‡</sup>, Isei Tanida<sup>‡</sup>, Tomoki Chiba<sup>§</sup>, Keiji Tanaka<sup>§</sup>, and Eiki Kominami<sup>‡2</sup>

From the <sup>‡</sup>Department of Biochemistry, Juntendo University School of Medicine, Bunkyo-ku, Tokyo 113-8421, the <sup>§</sup>Department of Molecular Oncology, Tokyo Metropolitan Institute of Medical Science, Bunkyo-ku, Tokyo 113-8613, and the <sup>¶</sup>Biology Laboratory, Interdisciplinary Graduate School of Medicine and Engineering, University of Yamanashi, Tamaho-machi, Yamanashi 409-38, Japan

Peroxisomes are degraded by autophagic machinery termed “pexophagy” in yeast; however, whether this is essential for peroxisome degradation in mammals remains unknown. Here we have shown that *Atg7*, an essential gene for autophagy, plays a pivotal role in the degradation of excess peroxisomes in mammals. Following induction of peroxisomes by a 2-week treatment with phthalate esters in control and *Atg7*-deficient livers, peroxisomal degradation was monitored within 1 week after discontinuation of phthalate esters. Although most of the excess peroxisomes in the control liver were selectively degraded within 1 week, this rapid removal was exclusively impaired in the mutant liver. Furthermore, morphological analysis revealed that surplus peroxisomes, but not mutant hepatocytes, were surrounded by autophagosomes in the control. Our results indicated that the autophagic machinery is essential for the selective clearance of excess peroxisomes in mammals. This is the first direct evidence for the contribution of autophagic machinery in peroxisomal degradation in mammals.

Reorganization of organelles constitutively or suddenly occurs in eukaryotic cells as an adaptation to environmental changes accompanying the cell cycle, development, and differentiation (1). Such alterations are stringently regulated by biogenesis and/or degradation. In the last decade, much attention was paid to the study of organelle assembly, an interest linked with the translocation of proteins into the organelles (2). One focus of that work was peroxisomes. Peroxisomes are single membrane-bound organelles that contribute to an array of metabolic pathways and are specifically and markedly induced by a group of non-genotoxic carcinogens and endogenous steroids in rodents (3–6). Indeed, peroxisome proliferators increase the size, number, and enzymes involved in fatty acid metabolism: e.g. peroxisomal thiolase (PT),<sup>3</sup> peroxisomal bifunctional protein (BF), and fatty acid  $\beta$ -oxidation of peroxisomes (7, 8). However, the mechanistic basis of peroxisome turnover remains poorly understood (8, 9).

In yeast species, such as *Pichia pastoris*, *Hansenula polymorpha*, *Candida boidinii*, and *Saccharomyces cerevisiae*, proliferating peroxisomes

are degenerated by an autophagy-related process named pexophagy during glucose or ethanol adaptation (10–14). Yeast genetics of pexophagy revealed that most autophagy-related (*Atg*) genes play indispensable roles in this selective degradation of peroxisomes as well as autophagy (8, 9, 13, 15, 16). In mammals, however, whether or not the autophagic machinery is involved in the degradation of excess peroxisomes biosynthesized in response to drug cues remains a mystery. In particular, there is no direct evidence for the degradation of disused peroxisomes by the autophagic machinery, and it is not clear whether such a degradation process, if any, is selective or non-selective. It has also been reported that selective degradation of mitochondria may occur via autophagy-related mechanism in yeast (17, 18). Therefore, selectivity in the organelle turnover via autophagy is an important issue.

Among the many *Atg* genes that regulate autophagy, *Atg7*, which encodes a ubiquitin-activating enzyme (E1)-like enzyme common to two ubiquitylation-like conjugations, the LC3 (*Atg8* in yeast) and Atg12 conjugation systems, is a critical gene for autophagosome formation in yeast and mammalian cells (19–26). It has been reported that in yeast, *Atg7/Apg7/Gsa7* is essential for pexophagy in addition to autophagy (19, 22, 24). During mammalian autophagy, LC3-I (a cytosolic form of LC3) is lipidated to LC3-II (its autophagosomal membrane-bound form) by *Atg7* (an E1-like enzyme) and *Atg3* (a ubiquitin carrier protein (E2)-like enzyme) (21, 27). Recently, we have established conditional knock-out mice of *Atg7* and have shown that *Atg7* is indispensable for mammalian autophagy and that the autophagy deficiency in liver leads to marked accumulation of cytoplasmic proteins (20). In the normal liver, LC3 is continuously synthesized to form LC3-I, and LC3-I is subsequently conjugated with phosphatidylethanolamine to form LC3-II during autophagy. LC3-II is then recruited to autophagosomal membranes (21, 28), and the autophagosomal LC3-II is rapidly degraded after fusion of autophagosome with lysosome (29). This dynamic flow of LC3 is completely inhibited in *Atg7*-deficient liver and, as a consequence, more LC3-I accumulates in the mutant liver (20). Considering that deletion of yeast *Atg7/Gsa7* gene results in a defect of pexophagy in *P. pastoris* (24), the liver-specific *Atg7*-conditional knock-out mice will be an advantageous tool in investigating the degradation of peroxisomes in mammals.

In this study, we analyzed the clearance of surplus peroxisomes using the conditional-knock-out mice of *Atg7* (20). The results indicated that autophagy is essential for the degradation of accumulated peroxisomes in the mouse liver.

## EXPERIMENTAL PROCEDURES

**Reagents**—Phthalate esters (diethylhexyl phthalate (DEHP)), corn oil, and leupeptin were purchased from Sigma.

\* This work was supported by Grants-in-aid 15032263, 16790195, 15590254, 09680629, and 1270040 from the Ministry of Education, Culture, Sports, Science and Technology of Japan. The costs of publication of this article were defrayed in part by the payment of page charges. This article must therefore be hereby marked “advertisement” in accordance with 18 U.S.C. Section 1734 solely to indicate this fact.

<sup>1</sup> Both authors contributed equally to this work.

<sup>2</sup> To whom correspondence should be addressed: Dept. of Biochemistry, Juntendo University School of Medicine, 2-1-1 Hongo, Bunkyo-ku, Tokyo 113-8421, Japan. Tel.: 81-3-5802-1031; Fax: 81-3-5802-5889; E-mail: komillabo@med.juntendo.ac.jp.

<sup>3</sup> The abbreviations used are: PT, peroxisomal thiolase; BF, bifunctional protein; DEHP, diethylhexyl phthalate; MLP, mitochondrial/lysosomal/peroxisomal; Atg, autophagy-related; BIP, binding protein; plpC, polyinosinic acid-polycytidylic acid.



## Selective Degradation of Excess Peroxisomes

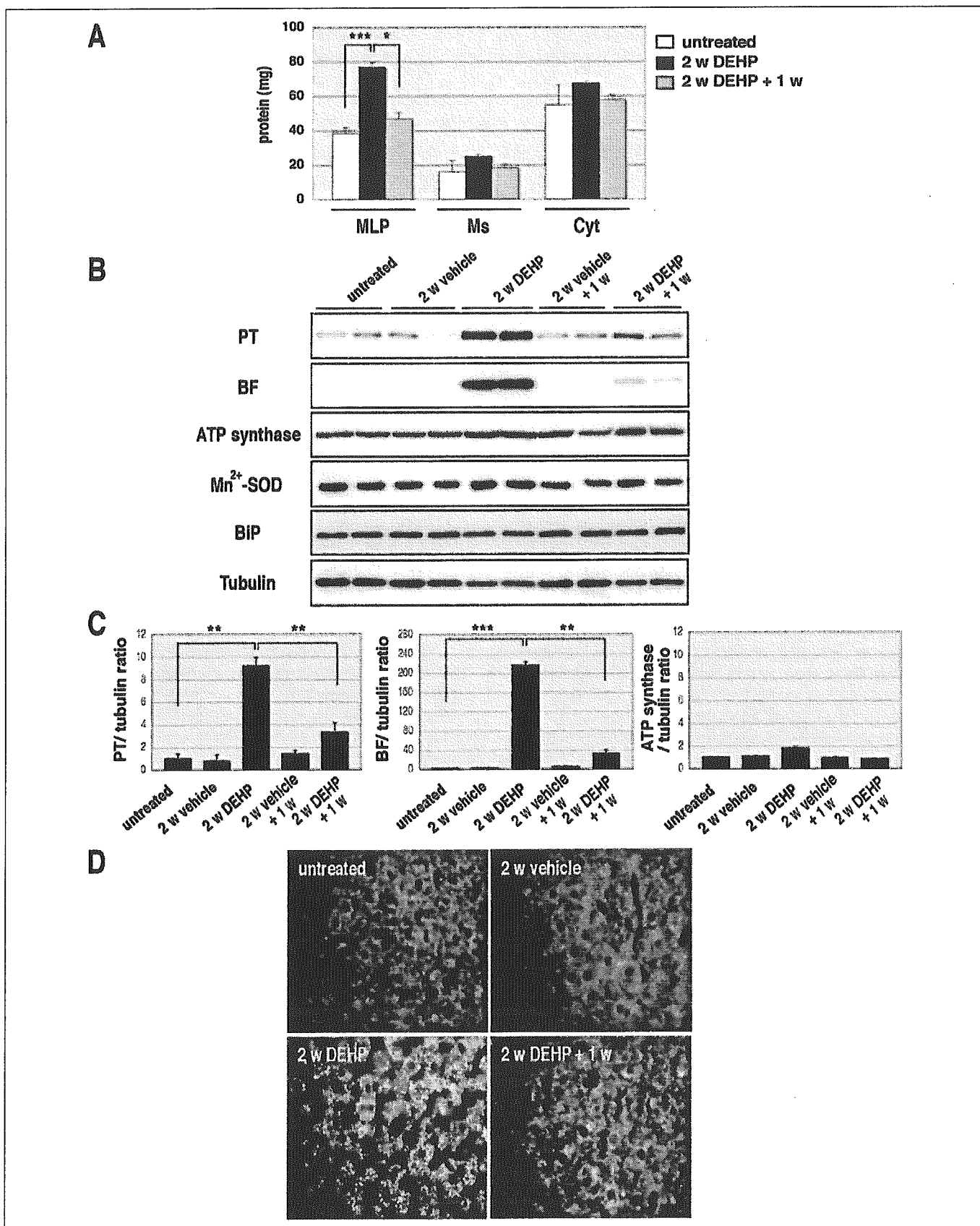


FIGURE 1. The recovery process of excess peroxisomes induced by DEHP treatment. *A*, wild-type mice were treated with DEHP for 2 weeks (*2 w DEHP*) and then chased for 1 week (*2 w DEHP + 1 w*). Untreated and treated mice were dissected, and liver homogenates were fractionated into MLP, microsomal (*Ms*), and cytosolic (*Cyt*) fractions. The protein amount in each fraction was measured. Data are mean  $\pm$  S.D. values of five mice in each group; \*,  $p < 0.02$  and \*\*\*,  $p < 0.001$ . *B*, wild-type mice were treated as described in *A*. The vehicle

**Animals and Treatment Regimen**—C57B6J mice were used as wild-type mice. Male mice received DEHP (1,150 mg/kg/day) or vehicle (corn oil, 5 ml/kg/day) via sonde daily for 2 weeks, and the mice were subsequently fed on a normal diet for 1 week to investigate the changes in proliferated peroxisomes during the recovery process according to the protocol reported previously (7). For detection of autophagosomes by electron microscopy, mice were injected with leupeptin (2 mg/100 g of body weight) after administration of DEHP. All animals were sacrificed by deep anesthesia.

**Deletion of *Atg7* in Mouse Liver**—*Atg7* conditional knock-out mice and the heterozygotes were prepared as described previously (20). Briefly, creatine expression in the liver was induced by intraperitoneal injection of polyinosinic acid-polycytidylic acid (pIpC). pIpC was injected three times at a 48-h interval.

**Preparation of the Fractions**—Livers from *Atg7<sup>F/F</sup>*:Mx1 and *Atg7<sup>F/F</sup>*:Mx1 mice were treated with DEHP or corn oil for 2 weeks, and at 1 week after treatment, they were dissected. Subfractionation of the livers was accomplished by differential centrifugation according to the method of de Duve *et al.* (30). Briefly, 20% homogenates were prepared in 0.25 M sucrose, 10 mM HEPES-NaOH, pH 7.4 (homogenizing buffer). The homogenate of the liver was centrifuged at  $650 \times g$  for 5 min to remove nuclei and unbroken cells. The pellets were resuspended in the same volume of homogenizing buffer and were then centrifuged. The supernatants from these two centrifugations were combined and used as postnuclear supernatant fractions. Postnuclear supernatant fractions were centrifuged at  $10,000 \times g$  for 20 min, and pellets were used as the mitochondrial/lysosomal/peroxisomal (MLP) fractions. The post-MLP supernatants were further centrifuged at  $105,000 \times g$  for 60 min to precipitate microsomal fractions in pellet form. All procedures were performed at 4 °C.

**Immunoblot Analysis**—Immunoblotting was performed as described previously (19). The antibody against  $Mn^{2+}$ -superoxide dismutase was kindly provided by Prof. Naoyuki Taniguchi (Osaka University, Japan). The antibodies for *Atg7* (19), LC3 (20), BF (31), PT (32), and the  $\beta$ -subunit of ATP synthase (33) were prepared as described previously. The antibodies against tubulin and BiP were purchased from Chemicon International, Inc. (Temecula, CA) and Affinity BioReagents, Inc. (Golden, CO), respectively.

**Histological Examination**—Livers were dissected, fixed in 4% paraformaldehyde, frozen, embedded, and sectioned. For immunohistochemical analysis, the sections were blocked with 5% normal goat serum in phosphate-buffered saline containing 0.2% Triton X-100 and then incubated with anti-PT antibody and Alexa Fluor 488-labeled second antibody (Molecular Probes, Eugene, OR). Fluorescence images were obtained using a fluorescence microscope (Q550FV; Leica, Germany) equipped with cooled charge-coupled device camera (CTR MIC; Leica). Pictures were taken using Leica Qfluoro software (Leica).

**Electron Microscopy**—Livers were perfusion-fixed with the fixative through the portal vein for 10 min. The fixative consisted of 2% paraformaldehyde, 1% glutaraldehyde, and 0.1 M HEPES-KOH buffer (pH 7.4). To visualize peroxisomes, some liver slices were incubated in alkaline 3,3-diaminobendine medium consisting of 2 mg/ml 3,3-diaminobendine, 0.02% hydrogen peroxide, and 0.2 M glycine-NaOH buffer (pH 10.0) for 1 h at room temperature. Then they were postfixed with 1% reduced osmium tetroxide for 1 h. The other tissue slices were post-

fixed in 1% reduced osmium tetroxide with 3,3-diaminobendine reaction. All tissue slices were then dehydrated in graded series of ethanol and embedded in Epon. Thin sections were cut with a diamond knife using an ultramicrotome (Reichert, Vienna, Austria). Sections were contrasted with 40 mM lead citrate for 5 min and examined with a Hitachi H7500 electron microscope (Hitachi, Tokyo, Japan).

**Quantitative Analysis of Peroxisomes**—For each tissue slice, 20 digital electron micrographs were acquired at  $\times 5,000$  magnification, enlarged 2.7-fold, and printed by a laser printer. Using the printed figure, we measured the area of peroxisomes and that of the cytoplasmic area of hepatocytes using a SigmaScan scientific measurement system equipped with a computer (Jandel Scientific, San Rafael, CA). The relative total area of peroxisomes was calculated using the following formula: (number of peroxisomes in the average area of peroxisomes/cytoplasmic area) and expressed in  $\mu m^2/100 \mu m^2$  of cytoplasmic area.

**Statistical Analysis**—The statistical significance of differences between experimental and control groups was determined by the two-tailed Student's *t* test. A *p* value of  $<0.05$  was considered statistically significant.

## RESULTS

**Selective Degradation of Excess Peroxisomes**—Phthalate ester (DEHP) and its active metabolite mono-ethylhexyl phthalate can cause marked increases in both the size and the number of peroxisomes and induce peroxisomal enzymes in the liver (7). Utilizing these phenomena, we first investigated the specific proliferation of peroxisomes and the rapid recovery after removal of the drugs in mice. Wild-type mice were treated with DEHP for 2 weeks and then chased for 1 week as described under "Experimental Procedures." The mice were dissected at each period, and the liver cell lysates were fractionated into MLP, microsomal, and cytosolic fractions. DEHP administration for 2 weeks was associated with about 2-fold increase in the amount of total protein in MLP, but not in microsomal or cytosolic fractions, as compared with untreated mice, and the amount almost returned to the basal level at 1 week after discontinuation of DEHP (Fig. 1A). These changes were not observed in mice treated with the vehicle (data not shown). Quantitative densitometric analysis of immunoblotting data revealed that PT and BF, marker proteins of peroxisomes, increased significantly after administration of DEHP but not the vehicle, and both diminished significantly to basal levels at 1 week after DEHP discontinuation (Fig. 1, B and C). In comparison, the levels of mitochondrial proteins, the  $\beta$ -subunit of ATP synthase and manganese superoxide dismutase, and the endoplasmic reticulum marker, BiP, remained unchanged during the same manipulations (Fig. 1B). Immunofluorescence analysis using anti-PT antibody revealed that a 2-week administration of DEHP, but not the vehicle, resulted in the appearance of numerous dots representing peroxisomes, and most of these dots disappeared at 1 week after discontinuation of DEHP (Fig. 1D). Considered together, these results indicate that DEHP-induced peroxisomes are selectively degraded following removal of the peroxisome proliferator.

**Impairment of Degradation of Proliferated Peroxisomes in Autophagy-deficient Liver**—Next, to examine the effects of autophagy deficiency on peroxisome degradation, we took advantage of the conditional knock-out mice, *Atg7<sup>F/F</sup>*:Mx1 (mutant mice), and their littermates, *Atg7<sup>F/+</sup>*:Mx1 mice (control mice), the systems of which

control mice were treated with corn oil for 2 weeks (2 w vehicle). Untreated and treated mice were sacrificed, and the livers were dissected out and homogenized, and then the postnuclear supernatant fractions were subjected to immunoblotting with anti-PT, BF,  $\beta$ -subunit ATP synthase,  $Mn^{2+}$ -superoxide dismutase (SOD), BiP, and tubulin antibodies. Tubulin was used as a control. Data shown are representative of three separate experiments. C, quantitative densitometry of immunoblotting data in B was performed, and the ratios between each of PT, BF, and ATP synthase and tubulin were plotted; \*\*,  $p < 0.01$ , \*\*\*,  $p < 0.001$ . D, wild-type mice were treated with DEHP as described in A, and the frozen sections of livers were stained with anti-PT antibody to detect peroxisomes. Magnification,  $\times 400$ .

## Selective Degradation of Excess Peroxisomes

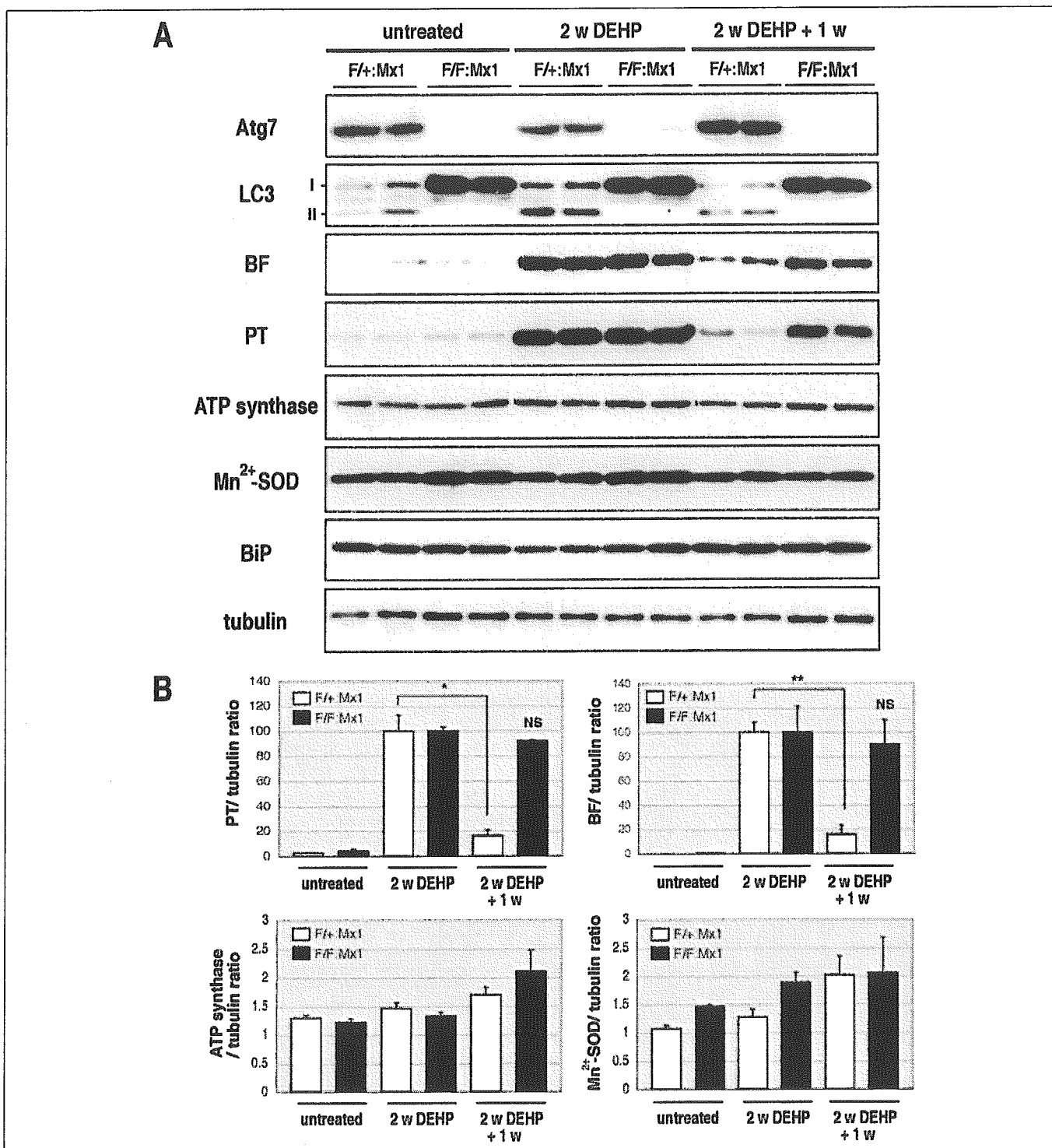


**FIGURE 2. The recovery process of excess peroxisomes is impaired in *Atg7*-deficient liver.** *A*, *Atg7*<sup>F/+</sup>;Mx1 (*F/+;Mx1*) and *Atg7*<sup>F/F</sup>;Mx1 (*F/F;Mx1*) mice were treated with DEHP for 2 weeks (2 w DEHP) and then chased for 1 week (2 w DEHP + 1 w). Both genotype mice were sacrificed at each time point. The liver was dissected out and homogenized, and then the postnuclear supernatant fractions were subjected to immunoblotting using anti-Atg7, LC3, BF, PT,  $\beta$ -subunit ATP synthase, Mn<sup>2+</sup>-superoxide dismutase (SOD), BiP, and tubulin antibodies. Tubulin was used as control. Data shown are representative of three separate experiments. *B*, quantitative densitometry of Western blotting shown in *A* was performed, and PT/tubulin, BF/tubulin,  $\beta$ -subunit ATP synthase/tubulin, and Mn<sup>2+</sup>-superoxide dismutase/tubulin ratios were plotted; \*,  $p < 0.02$ , \*\*,  $p < 0.01$ , NS; not significant.

were recently established by our group (20). Autophagy is impaired following plpC injection in *Atg7*<sup>F/F</sup>;Mx1 mouse livers. Indeed, we verified that Atg7 protein deletion in *Atg7*<sup>F/F</sup>;Mx1 but not *Atg7*<sup>F/+</sup>;Mx1 livers was plpC injection-dependent (Fig. 2A). Furthermore, we also tested the loss of Atg7 activity by investigating the lack of LC3-II (a

membrane-bound form of LC3) and accumulation of LC3-I (a cytosolic form of LC3) in the liver. It is generally accepted that LC3-II is a marker protein of autophagosomal membranes (21). Although both forms were detected in the control liver, only LC3-I accumulated in the mutant liver (Fig. 2A), indicating impairment of autophagy in mutant *Atg7*<sup>F/F</sup>;Mx1

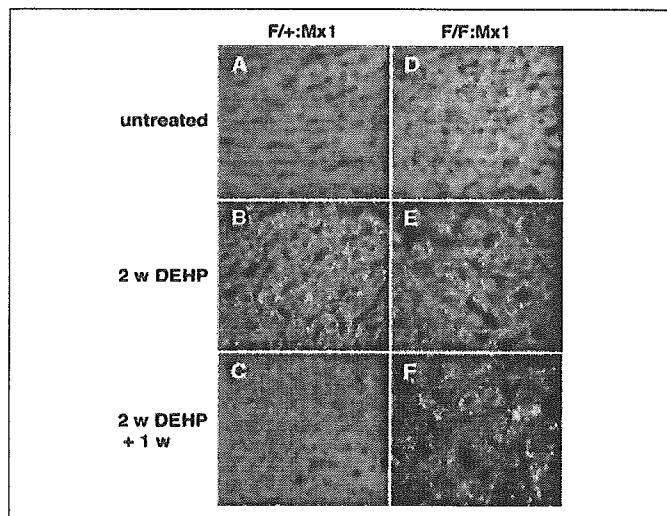


**FIGURE 3. Accumulation of excess peroxisomes in *Atg7*-deficient liver.** Immunofluorescent detection of peroxisomes with anti-PT antibody in the *Atg7*<sup>F/+</sup>;Mx1 (A–C, F/+;Mx1) and *Atg7*<sup>F/F</sup>;Mx1 (D–F, F/F;Mx1) liver is shown. *Atg7*<sup>F/+</sup>;Mx1 and *Atg7*<sup>F/F</sup>;Mx1 mice were treated with DEHP for 2 weeks (B and E, 2 w DEHP) and then chased for 1 week (C and F, 2 w DEHP + 1 w). Untreated (A and D) and treated mice were sacrificed, and the livers were isolated. The frozen sections of livers were immunostained with anti-PT antibody. Magnification,  $\times 400$ .

mouse liver (20). In the control livers, although LC3-II were induced by the proliferated peroxisomes (Fig. 2A, indicated by 2 w DEHP), it was decreased almost to the basal levels at 1 week after withdrawal of DEHP (Fig. 2A), suggesting that autophagy was induced to remove surplus peroxisomes. After a 2-week treatment with DEHP, the livers were dissected, and total proteins in the lysates of mutant and control livers were separated by SDS-PAGE and subjected to immunoblot analyses. Similar to the results obtained with wild-type mice (Fig. 1), BF and PT increased profoundly after the treatment as compared with mice prior to DEHP administration and then decreased almost to the basal levels at 1 week after discontinuation in *Atg7*<sup>F/+</sup>;Mx1 livers (Fig. 2, A and B). Although this increase was also detected in mutant *Atg7*<sup>F/F</sup>;Mx1 livers, the increased PT and BT proteins did not return to the basal levels following the discontinuation of DEHP (Fig. 2, A and B). In contrast to peroxisomal proteins, the levels of mitochondrial ( $\beta$ -subunit of ATP synthase and Mn<sup>2+</sup>-superoxide dismutase) and endoplasmic reticulum (BiP) markers did not change under these conditions (Fig. 2, A and B). These results indicate selective impairment of degradation of excess peroxisomal proteins in autophagy-deficient *Atg7*<sup>F/F</sup>;Mx1 liver.

We further confirmed the impairment of peroxisome degradation in autophagy-deficient liver by immunofluorescence analysis using anti-PT antibody (Fig. 3). The PT-positive dots representing peroxisomes were markedly increased following a 2-week DEHP treatment in both genotype livers, as compared with untreated mice (Fig. 3, A and D versus B and E). Although the dots almost disappeared to the basal levels at 7 days after discontinuation of DEHP in the control (Fig. 3C), most of the peroxisome dots remained visible in mutant liver after the same intervention (Fig. 3F). The data are in agreement with the biochemical results shown in Fig. 2. Based on these results, we concluded that autophagy is essential for selective degradation of excess peroxisomes.

**Engulfment of Excess Peroxisomes by Autophagosomal Membranes in Control Hepatocytes**—Finally, we used electron microscopy to explore the level of the peroxisomes in *Atg7*<sup>F/F</sup>;Mx1 and *Atg7*<sup>F/+</sup>;Mx1 livers (Fig. 4). Consistent with the results of immunofluorescent analysis, numerous peroxisomes were detected following a 2-week DEHP treatment in both wild and mutant hepatocytes (Fig. 4, B and E), and most of these

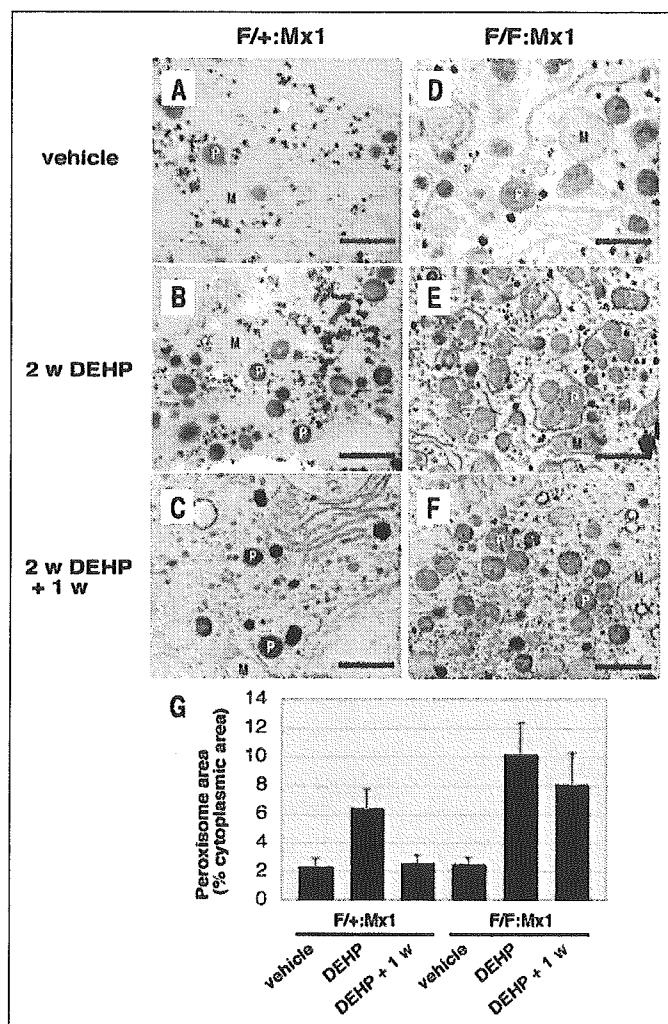


**FIGURE 4. Electron microscopic evaluation of livers of *Atg7*-deficient mice treated with DEHP.** A–F, electron micrographs of the liver of representative *Atg7*<sup>F/+</sup>;Mx1 mice (F/+;Mx1) and *Atg7*<sup>F/F</sup>;Mx1 (F/F;Mx1) mice treated with DEHP for 2 weeks (B and E, 2 w DEHP) and then fed on normal diet for 1 week (C and F, 2 w DEHP + 1 w). The vehicle control mice of each genotype were treated with corn oil for 2 weeks (A and D). The hepatocytes of both genotypes contained a high number of peroxisomes (P) after DEHP treatment (B and E). Note that induced peroxisomes were retained at 1 week after discontinuation of DEHP in *Atg7*<sup>F/F</sup>;Mx1 hepatocytes, in contrast to the decreased number in *Atg7*<sup>F/+</sup>;Mx1 hepatocytes (C and F). Bars, 1  $\mu$ m. The total area of peroxisomes relative to the cytoplasmic area was determined in each genotype ( $n = 10$ ). M, mitochondria; G, morphometric analysis of peroxisomes in *Atg7*<sup>F/+</sup>;Mx1 and *Atg7*<sup>F/F</sup>;Mx1 mice.

structures disappeared after 1 week of discontinuation of DEHP in the control, but not mutant, hepatocytes (Fig. 4, C and F). The relative total area of peroxisomes was determined, and the mean values are shown in Fig. 4G. Although the relative total area of peroxisomes increased in both groups after a 2-week DEHP administration, the area decreased to the basal level in control hepatocytes, but not in mutant hepatocytes, at 1 week after DEHP withdrawal from the diet (Fig. 2G).

After discontinuation of DEHP, we detected only a few autophagosome-like structures in control hepatocytes, probably due to the rapid turnover of autophagosomes by lysosome (Fig. 4C). Considering the selective degradation of peroxisomal marker proteins, PT and BF (Fig. 2), autophagosomes that selectively enwrap peroxisomes could be observed by electron microscopic analysis when lysosomal proteolysis is inhibited. Therefore, we examined whether proliferated peroxisomes enclosed by autophagosomal membranes can be detected under the condition of inhibited autophagic proteolysis. Injection of leupeptin, a



## Selective Degradation of Excess Peroxisomes

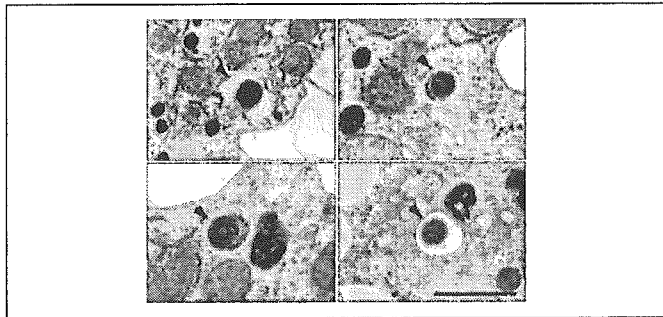


FIGURE 5. Excess peroxisomes are surrounded by autophagosome. *Atg7<sup>Fl/+</sup>*:Mx1 mice were treated with DEHP for 2 weeks and then injected with leupeptin as described under "Experimental Procedures." The mice were sacrificed, and the livers were dissected out and processed for electron microscopic examination. These images show representative autophagosomes surrounding peroxisomes. Four typical electron micrographs are represented. Arrowheads indicate the engulfment of peroxisome(s) by isolated membranes. Bars, 1  $\mu$ m.

lysosomal cysteine proteinase inhibitor, into a 2-week DEHP-treated control *Atg7<sup>Fl/+</sup>*:Mx1 mouse resulted in marked accumulation of autophagosomes, and some peroxisomes were surrounded by a double-membrane structure, autophagosome, in control hepatocytes (Fig. 5). No autophagosome was identified in hepatocytes of *Atg7<sup>Fl/F</sup>*:Mx1 mice (data not shown). These lines of evidence indicated that the autophagic machinery mediated is essential for selective clearance of excess peroxisomes, as it is so for starvation-induced autophagy in the mouse liver.

### DISCUSSION

Most cellular components, if not all, are regulated quantitatively to maintain cell homeostasis. For this regulation, there are growing lines of evidence for the importance of the balance between biosynthesis and degradation. Peroxisomes, a typical cellular component, are dynamic organelles induced and degraded in response to extracellular cues (8). However, little is known about the mechanism for peroxisome degradation in mammals. There are two major concepts for degradation of peroxisomes, *i.e.* autophagic machinery and autolysis (34, 35). By the analysis of autophagy-deficient livers, we showed the first direct evidence that peroxisomal breakdown is mainly, if not entirely, dependent on autophagic machinery. Based on quantitative densitometry with two peroxisome marker enzymes (Fig. 2, PT and BF) as well as morphometry of the electron micrographs (Fig. 4), ~70–80% of peroxisomes induced by DEHP were degraded via autophagy during 1 week after discontinuation of the drug administration.

Considering peroxisome degradation by autophagic machinery in mammals, it is important to know whether the process occurs via micropexophagy or macropexophagy. In methylotrophic yeast species, it is well established that the autophagy-related process, termed pexophagy, induces a rapid and selective degradation of excess peroxisomes (13). In *P. pastoris* cells, following a shift from methanol to ethanol or glucose, unnecessary peroxisomes are degraded by macropexophagy and micropexophagy, respectively (9). Macropexophagy is the degradation pathway in which autophagosomes selectively surround excess peroxisomes. On the other hand, in micropexophagy, the excess peroxisomes are not degraded through autophagosome formation. The initial step in micropexophagy is invagination and septation of a vacuole followed by engulfment of the peroxisomes by the vacuole. In the final stage, the edges of the vacuole fuse with each other followed by vacuolar degradation of the peroxisomal membrane and its contents. Because *ATG7* is essential for both macropexophagy and micropexophagy in *P. pastoris* cells, it is plausible that excess peroxisomes in mammalian cells are also degraded by both macroautophagy and

micropexophagy. Our data using electron microscopy revealed that autophagosomes preferentially surrounded excess peroxisomes in control hepatocytes (Fig. 5), suggesting that DEHP-induced peroxisomes are degraded mainly through the process of macropexophagy. Thus, we could show the selective role of autophagic machinery in the clearance of surplus peroxisomes after induction of peroxisomes by phthalate esters.

Recent studies provided evidence for the involvement of the autophagic machinery in selective sequestration of proteins in the cell. For example, the precursor form of aminopeptidase I (prApe1) is a selective cargo molecule of autophagy in yeast (36), and cytosolic acetaldehyde dehydrogenase (Ald6p) is preferentially transported to vacuoles via autophagosomes in yeast (37). Consistently, the autophagic machinery could also selectively eliminate pathogenic group A *Streptococci* invading the cells (38). These reports strongly suggest that autophagosomes sequester the cytosolic protein(s) and invading pathogens in a highly selective manner. We recently reported that *Atg7*-deficient hepatocytes exhibit impaired constitutive autophagy responsible for selective degradation of ubiquitinated proteins (20). Our previous findings together with the present results suggest that the autophagic process eliminates abnormal and/or excess proteins and organelles including peroxisomes in a selective manner even under normal conditions. How the autophagy machinery recognizes these organelles to degrade them awaits further investigation.

*Acknowledgment*—We thank Tsuguko Kouno for technical assistance.

### REFERENCES

1. Lazarow, P. B., and Fujiki, Y. (1985) *Annu. Rev. Cell Biol.* **1**, 489–530
2. Heiland, I., and Erdmann, R. (2005) *FEBS J.* **272**, 2362–2372
3. Reddy, J. K., Azarnoff, D. L., Hignite, C. E. (1980) *Nature* **283**, 397–398
4. Reddy, J. K., Lalwani, N. D. (1983) *CRC Crit. Rev. Toxicol.* **12**, 1–58
5. Nicholls-Grzemski, F. A., Calder, I. C., and Priestly, B. G. (1992) *Biochem. Pharmacol.* **7**, 1395–1396
6. Vanden Havel, J. P. (1999) *Toxicol. Sci.* **47**, 1–8
7. Yokota, S. (1993) *Eur. J. Cell Biol.* **61**, 67–80
8. Subramani, S. (1998) *Physiol. Rev.* **78**, 171–188
9. Farre, J. C., and Subramani, S. (2004) *Trends Cell Biol.* **14**, 515–523
10. Kim, J., Kamada, Y., Stromhaug, P. E., Guan, J., Hefner-Gravink, A., Baba, M., Scott, S. V., Ohsumi, Y., Dunn, W. A., Jr., and Klionsky, D. J. (2001) *J. Cell Biol.* **153**, 381–396
11. Stromhaug, P. E., Bevan, A., and Dunn, W. A., Jr. (2001) *J. Biol. Chem.* **276**, 42422–42435
12. Bellu, A. R., Komori, M., Klei, I. J., Kiel, J. A., and Veenhuis, M. (2001) *J. Biol. Chem.* **276**, 44570–44574
13. Bellu, A. R., and Kiel, J. A. (2003) *Microsc. Res. Tech.* **61**, 161–170
14. Ano, Y., Hattori, T., Oku, M., Mukaiyama, H., Baba, M., Ohsumi, Y., Kato, N., and Sakai, Y. (2005) *Mol. Biol. Cell* **16**, 446–457
15. Klionsky, D. J., and Ohsumi, Y. (1999) *Annu. Rev. Cell Dev. Biol.* **15**, 1–32
16. Kim, J., and Klionsky, D. J. (2000) *Annu. Rev. Biochem.* **69**, 303–342
17. Kissova, I., Deffieu, M., Manon, S., and Camougrand, N. (2004) *J. Biol. Chem.* **279**, 39068–39074
18. Lemasters, J. J. (2005) *Rejuvenation Res.* **8**, 3–5
19. Tanida, I., Mizushima, N., Kiyooka, M., Ohsumi, M., Ueno, T., Ohsumi, Y., and Kominami, E. (1999) *Mol. Biol. Cell* **10**, 1367–1379
20. Komatsu, M., Waguri, S., Ueno, T., Iwata, J., Murata, S., Tanida, I., Ezaki, J., Mizushima, N., Ohsumi, Y., Uchiyama, Y., Kominami, E., Tanaka, K., and Chiba, T. (2005) *J. Cell Biol.* **169**, 425–434
21. Kabeya, Y., Mizushima, N., Ueno, T., Yamamoto, A., Kirisako, T., Noda, T., Kominami, E., Ohsumi, Y., and Yoshimori, T. (2000) *EMBO J.* **19**, 5720–5728
22. Mizushima, N., Noda, T., Yoshimori, T., Tanaka, Y., Ishii, T., George, M. D., Klionsky, D. J., Ohsumi, M., and Ohsumi, Y. (1998) *Nature* **395**, 395–398
23. Ichimura, Y., Kirisako, T., Takao, T., Satomi, Y., Shimonishi, Y., Ishihara, N., Mizushima, N., Tanida, I., Kominami, E., Ohsumi, M., Noda, T., and Ohsumi, Y. (2000) *Nature* **408**, 488–492
24. Yuan, W., Stromhaug, P. E., and Dunn, W. A., Jr. (1999) *Mol. Biol. Cell* **10**, 1353–1366
25. Tanida, I., Tanida-Miyake, E., Ueno, T., and Kominami, E. (2001) *J. Biol. Chem.* **276**, 1701–1706

26. Tanida, I., Tanida-Miyake, E., Nishitani, T., Komatsu, M., Yamazaki, H., Ueno, T., and Kominami, E. (2002) *Biochem. Biophys. Res. Commun.* **292**, 256–262
27. Tanida, I., Tanida-Miyake, E., Komatsu, M., Ueno, T., and Kominami, E. (2002) *J. Biol. Chem.* **277**, 13739–13744
28. Asanuma, K., Tanida, I., Shirato, I., Ueno, T., Takahara, H., Nishitani, T., Kominami, E., and Tomino, Y. (2003) *FASEB J.* **17**, 1165–1167
29. Tanida, I., Minematsu-Ikeguchi, N., Ueno, T., and Kominami, E. (2005) *Autophagy* **1**, 84–91
30. de Duve, C., Pressman, B. C., Gianetto, R., Wattiaux, R., and Appelmans, F. (1955) *Biochem. J.* **60**, 604–617
31. Usuda, N., Yokota, S., Ichikawa, R., Hashimoto, T., and Nagata, T. (1991) *J. Histochem. Cytochem.* **39**, 95–102
32. Tsukamoto, T., Yokota, S., and Fujiki, Y. (1990) *J. Cell Biol.* **110**, 651–660
33. Ezaki, J., Wolfe, L. S., Higuti, T., Ishidoh, K., and Kominami, E. (1995) *J. Neurochem.* **64**, 733–741
34. Yokota, S., Oda, T., and Fahimi, H. D. (2001) *J. Histochem. Cytochem.* **49**, 613–621
35. Yokota, S. (2003) *Microsc. Res. Tech.* **61**, 151–160
36. Shintani, T., and Klionsky, D. J. (2004) *J. Biol. Chem.* **279**, 29889–29894
37. Onodera, J., and Ohsumi, Y. (2004) *J. Biol. Chem.* **279**, 16071–16076
38. Nakagawa, I., Amano, A., Mizushima, N., Yamamoto, A., Yamaguchi, H., Kamimoto, T., Nara, A., Funao, J., Nakata, M., Tsuda, K., Hamada, S., and Yoshimori, T. (2004) *Science* **306**, 1037–1040

